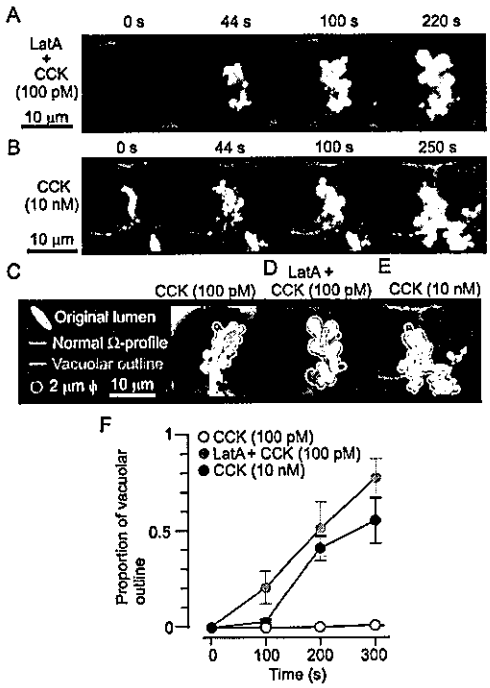

FIG. 4. **Real-time imaging of vacuole formation.** *A* and *B*, SRB fluorescence images, both of an acinus treated with 10 μM LatA for 30 min before stimulation for the indicated times with 100 pM CCK (*A*) and of an acinus stimulated with 10 nM CCK (*B*). See Supplementary Movies 2 and 3 for real-time movies corresponding to these images. *C–E*, vacuolar outlines (*blue*) and normal Ω-shaped profiles (*white*) among newly formed lumens in acini pretreated (*D*) or not (*C*) with LatA before stimulation with 100 pM CCK or in an acinus stimulated with 10 nM CCK (*E*). The images correspond to those shown in Fig. 1*C* (220 s) and in *panels A* (220 s) and *B* (250 s) of this figure, respectively. The *circle* in *C* has a diameter of 2 μm, above or below which an outline was classified as vacuolar or normal (Ω-profile). The original lumen is shown in *green*. *F*, the time courses of the formation of vacuoles estimated from the vacuolar portion of luminal outlines in acini treated as in *C–E*. Data are means ± S.E. (n = 6–16 cells).

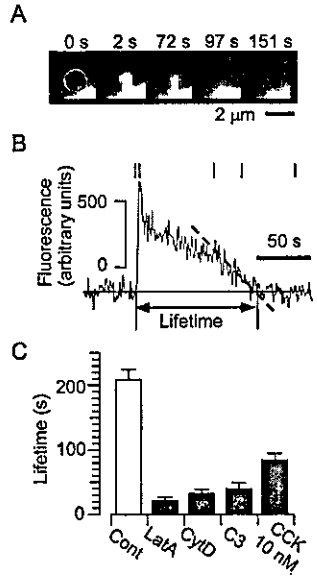

FIG. 5. **Effects of F-actin coating on the stability of Ω-shaped profiles.** *A*, SRB fluorescence images of an Ω-shaped profile formed by a granule that underwent exocytosis at the apical membrane in a cell stimulated with 100 pM CCK. *B*, changes in the SRB fluorescence intensity of the Ω-shaped profile indicated by the *blue circle* in *A*. The *vertical lines* indicate the times of acquisition of the images in *A*. The lifetime of Ω-profiles was determined by straight-line fitting of the last 20 s of the decay in fluorescence (*dotted line*). *C*, lifetimes of Ω-shaped profiles in acini stimulated with 100 pM CCK (*Cont*) without or with pretreatment with LatA (10 μM, 30 min), cytochalasin D (*CytD*, 10 μM, 30 min), or exoenzyme C3 (50 μg ml^{-1}, 2 h) and in those stimulated with CCK 10 nM without any pretreatments. Data are means ± S.E. of values from 95, 88, 75, 32, and 35 Ω-shaped profiles, respectively.

was thus substantially reduced in acini treated with 10 μM LatA for 30 min without agonist stimulation (288 ± 19 arbitrary units; mean ± S.E., n = 11 cells, $p < 0.01$) (Fig. 3*E*) as compared with that in control acini (1192 ± 52 arbitrary units, n = 18) (Fig. 1*D*). In contrast, treatment of acini for 2 h with exoenzyme C3 (50 μg ml^{-1}) did not result in a marked reduction in F-actin coating at the apical membrane (Fig. 3*F*). The fluorescence intensity of Alexa 488-phalliodin at the apical membrane in such acini (1238 ± 81 arbitrary units, n = 12 cells) did not differ significantly from that in control acini ($p >$ 0.05). Exposure of cultured acini to exoenzyme C3 for 3 days, however, almost completely eliminated the F-actin coat at the apical membrane (58 ± 6 arbitrary units; mean ± S.E., n = 24) as compared with that in control cultured cells (982 ± 109 arbitrary units, n = 13) without reducing the abundance of G-actin in the cytosol, as revealed by staining with Texas red-conjugated DNase I (Fig. 3, *G* and *H*). Rho-dependent actin polymerization thus occurs at the apical membrane but at a slow rate, and it might be activated in the granule membrane after exocytosis (see "Discussion").

Real-time Imaging of Vacuole Formation—We next investigated the formation of vacuoles by real-time imaging of acini immersed in a solution containing SRB. Vacuole formation was rarely detected in acini (<3%, n = 90 cells) stimulated with 100 pM CCK for up to 10 min (Fig. 1*C*). In contrast, abnormal round vacuoles with a diameter of >2 μm were formed by the merger of fused granules within 100 s after stimulation with 100 pM CCK in 93% of acini (n = 29 cells) that had been pretreated with LatA (10 μM) for 30 min (Fig. 4*A*; see Supplementary Movie 2). The vacuoles subsequently expanded, exhibiting mean diameters of 2.4 ± 0.1 (mean ± S.E., n = 13) and 4.6 ± 1.3 μm (n = 20) at 100 and 300 s after stimulation.

To quantify vacuole formation and expansion, we classified newly formed luminal profiles as vacuolar (spherical expanding structures with a maximal diameter of >2 μm) or normal (Ω-shaped) (Fig. 4, *C–E*). The proportion of vacuoles was estimated as $l_v/(l_n + l_v)$, where l_v and l_n are the lengths of vacuolar and normal outlines, respectively. The values were <2 and 78% in control and LatA-pretreated preparations, respectively, at 300 s after the onset of stimulation with 100 pM CCK (Fig. 4*F*). Pretreatment with other inhibitors of actin polymerization, including cytochalasin D (10 μM, 30 min) (28) and exoenzyme C3 (50 μg ml^{-1}, 2 h), also increased the proportion of vacuoles to 72% (n = 7 cells) and 38% (n = 6), respectively, at 300 s after stimulation with CCK (100 pM). The spherical and expanding nature of vacuoles suggests that the granule contents swelled within them and that F-actin coating prevents such swelling by stabilizing the Ω-shaped profiles.

The stability of Ω-profiles was directly quantified by measuring the lifetime of those formed by primary exocytic events that did not give rise to secondary exocytosis (Fig. 5*A*). Given that the time course of the flattening of the granule membrane into the plasma membrane was complex, we determined the lifetime of Ω-shaped profiles as the time required for their disappearance (Fig. 5*B*), which we estimated by straight-line fitting of the last 20 s of flattening (Fig. 5*B*). All three inhibitors of actin polymerization examined (LatA, cytochalasin D, exoenzyme C3) markedly reduced the lifetime of Ω-shaped profiles (Fig. 5*C*), supporting the notion that the profiles are stabilized by F-actin coating. The instability of Ω-shaped profiles is con-

sistent with the generation of vacuoles in LatA-pretreated cells because these treatments did not significantly reduce the incidence of sequential exocytosis, which was 71.6 ± 7.4% (mean ± S.E., n = 19 cells) and 72.8 ± 6.0% (mean ± S.E., n = 14) in control and LatA-pretreated preparations, respectively, and because the granules that induced sequential exocytosis did not flatten into the plasma membrane (see Supplementary Movies 1 and 2). In LatA-pretreated preparations, Ω-shaped profiles of the granules that were involved in sequential exocytosis were also instable and gave rise to vacuole formation.

As mentioned above, stimulation of acini with a high concentration (10 nM) of CCK alone triggered the generation of vacuoles (Fig. 4*B*; see Supplementary Movie 3). Indeed, the vacuolar proportion was 56% at 300 s after such stimulation (Fig. 4*F*), and the lifetime of primary Ω-profiles induced by stimulation with 10 nM CCK was reduced as compared with that of those elicited by stimulation with 100 pM agonist (Fig. 5*C*). A delay in the onset of vacuole formation was evident under such conditions, however, with the proportion of vacuoles being only 2.9% at 100 s after stimulation ($p < 0.005$) as compared with that in LatA-pretreated cells. These data suggest that stimulation of acini with a high concentration of CCK results in a slow destabilization of Ω-profiles, likely by impairment of the F-actin coating of granule membranes (Fig. 3*C*).

Importantly, vacuole formation was rarely observed in the acini (5%, n = 60 cells) stimulated by photolysis of a caged-Ca^{2+} compound in which micromolar increases in $[Ca^{2+}]_i$ persisted for more than 300 s (Fig. 2). The proportion of vacuole was less than 2% at 300 s after the stimulation. These data suggest that vacuole formation does not simply result from sustained increases in $[Ca^{2+}]_i$ but requires receptor activation.

Regulation of Exocytosis by F-actin Coating—Removal of the constitutive F-actin coat of the apical plasma membrane did not by itself trigger exocytosis, given that LatA alone did not induce exocytosis (data not shown). Moreover, the number of exocytic events in CCK-stimulated acini was not affected by pretreatment with LatA (Fig. 6, *A* and *B*). The number of exocytic events at the apical membrane (designated primary or first exocytosis; Fig. 6*A*) during stimulation with CCK (100 pM) for 10 min was thus not significantly ($p > 0.05$) affected by pretreatment of acini with LatA (10 μM) for 30 min (Fig. 6*B*), although the amount of F-actin at the apical membrane was markedly reduced by such LatA pretreatment (Fig. 3*E*). Furthermore, the number of secondary, tertiary, or quaternary exocytic events (second, third, or fourth exocytosis, respectively) (Fig. 6*A*) did not differ significantly between CCK-stimulated acini that had been pretreated with LatA and those that had not (Fig. 6*B*), although LatA completely inhibited the dynamic F-actin coating of granule membranes (Fig. 3, *A* and *B*). These results indicate that the size of the releasable pool of granules was not increased either by removal of the constitutive F-actin coat of the apical membrane or by prevention of the F-actin coating of granule membranes.

To quantify the rate of exocytosis, we defined the latency to primary exocytosis (L_1) as the time between the onset of the increase in $[Ca^{2+}]_i$ and the formation of the first Ω-shaped profile, and we have defined the latency to secondary (L_2) or tertiary (L_3) exocytic events as the time between the corresponding sequential fusion reactions (Fig. 6*A*). The rate of exocytosis induced by CCK (100 pM) was increased slightly by LatA pretreatment (Fig. 6*C*), with L_3 being significantly reduced by such pretreatment. It was possible, however, that LatA interfered with the agonist-evoked increase in $[Ca^{2+}]_i$ (29). To exclude this latter possibility, we triggered exocytosis by inducing a rapid and homogeneous increase in $[Ca^{2+}]_i$ through photolysis of NP-EGTA (Fig. 2*B*) (30). Under these

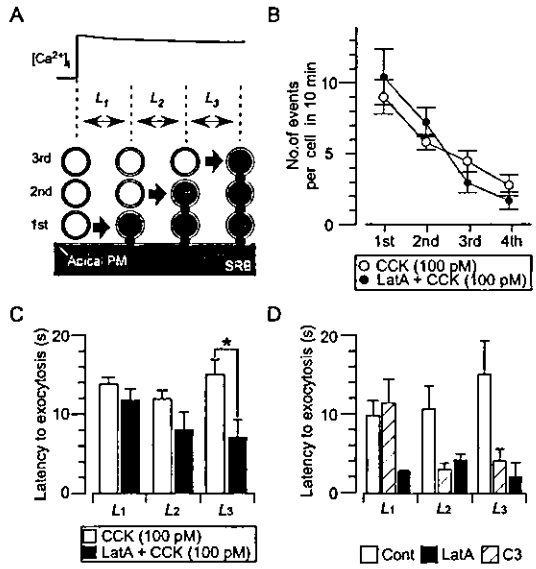

FIG. 6. **Effects of F-actin coating on the releasable pool of granules and on the latency of exocytosis.** *A*, definitions for latencies of first, second, and third exocytic events during sequential exocytosis. L_1 was defined as the time between the onset of the increase in $[Ca^{2+}]_i$ and that of the first exocytic event, whereas L_2 and L_3 were defined as the times between the onset of the first or second event and that of the second or third event, respectively. *PM*, plasma membrane. *B*, numbers of sequential exocytic events in acini stimulated with CCK (100 pM) for 10 min with (n = 14 cells) or without (n = 13) pretreatment with LatA (10 μM, 30 min). Data are means ± S.E. *C*, latencies for exocytic events visualized by SRB fluorescence during sequential exocytosis stimulated by CCK with or without pretreatment of acini with LatA. Data are means ± S.E. of values from 147, 91, 50, 22, 27, and 7 exocytic events for the *bars* from *left* to *right*, respectively. *, $p < 0.04$ (two-tailed Student's t test). *D*, latencies for exocytic events during sequential exocytosis induced by photolysis of NP-EGTA in acini pretreated or not with exoenzyme C3 (50 μg ml^{-1}, 2 h) or LatA (10 μM, 30 min). Data are means ± S.E. of values from 5 to 110 exocytic events visualized by SRB fluorescence. *Cont*, control.

conditions, latencies reflect the time required for membrane fusion after Ca^{2+} binding to the Ca^{2+} sensor of the granule (Fig. 6*A*). We found that L_1 was reduced by LatA but not by exoenzyme C3 (Fig. 6*D*), consistent with the reduction in the constitutive F-actin coating of the apical plasma membrane by LatA but not by exoenzyme C3 (Fig. 3, *E* and *F*). The constitutive F-actin coating of the plasma membrane thus increases the time required for membrane fusion after Ca^{2+} binding. In contrast, L_2 and L_3 were reduced by either LatA or exoenzyme C3 (Fig. 6*D*), consistent with the prevention by each agent of the dynamic F-actin coating of granules undergoing exocytosis (Fig. 3, *A*, *B*, and *D*). Given that granules are not coated with F-actin under resting conditions (Fig. 1*D*), these data indicate that dynamic actin polymerization regulates the fusion reaction.

DISCUSSION

With the use of two-photon microscopy, we have demonstrated that dynamic coating with F-actin occurs exclusively at the membranes of granules that are undergoing exocytosis in pancreatic acinar cells. It is likely that such F-actin coating is mediated by the polymerization of G-actin rather than by the lateral diffusion of F-actin from the apical plasma membrane, given that it was blocked by inhibitors of actin polymerization. The stability of the Ω-shaped profiles of fused granules is also consistent with the formation of a new F-actin coat by polymerization. Such coating occurs rapidly, given that most granules undergoing exocytosis were coated within 1 min after stimulation. In contrast to our conclusion, the F-actin coating

of zymogen granules was previously suggested to precede exocytosis (12); however, F-actin coating was examined 1 h after stimulation, F-actin-coated structures were sparse, and their origins were unclear in this previous study.

The selectivity of the F-actin coating of granules undergoing exocytosis might be achieved by the lateral diffusion of factors that promote actin polymerization from the apical membrane to the granule membrane. Indeed, actin-polymerizing activity appears to be associated with the apical membrane. Our observation that exoenzyme C3 prevented the rapid F-actin coating of granule membranes but did not affect the constitutive F-actin coating of the apical membrane suggests that Rho might be activated as a result of the mixing of plasma membrane and zymogen granule factors. The mixing of components of the granule and apical plasma membranes after exocytosis (31) and the lateral diffusion of an apical membrane protein and intramembrane particles into exocytic granules (32) have been demonstrated in freeze-fracture studies of the parotid gland. Candidates for plasma membrane factors that might diffuse into the granule membrane include RhoGEF (guanine nucleotide exchange factor for Rho) (33, 34), phosphatidylinositol 4,5-bisphosphate (35), and plectin (16, 36). Sequential exocytosis has also been proposed to be mediated by the lateral diffusion of apical membrane fusion proteins (10, 37).

Similar Cdc42-mediated coating of cortical granules with F-actin was recently described in *Xenopus* oocytes and was implicated in rapid endocytosis (38). In acinar cells, however, Ω-profiles persisted for several minutes before eventually merging with the lumen (Fig. 5*A*) and only infrequently underwent direct ("kiss-and-run") endocytosis. Thus, F-actin coating appears primarily to regulate Ω-profiles of granules and exocytosis in exocrine acinar cells.

We found that the rate of exocytosis of zymogen granules was reduced both by the constitutive F-actin coating of the apical membrane and by the dynamic F-actin coating of exocytic granules. These data support the classical notion that F-actin functions as a physical barrier to exocytosis (4–7). Prevention of F-actin polymerization did not increase the overall extent of exocytosis, however, indicating that F-actin coating reduced only the rate of fusion. Although the intensity of staining of the apical and granule membranes with fluorescent phalloidin was intense, F-actin coating might actually be sufficiently sparse to allow contact between proteins in these two membranes that mediate membrane fusion. F-actin coating may slow exocytosis by reducing the incidence of collision between such proteins in the opposing membranes. Slowing of exocytosis by the F-actin coating of the granule membrane likely in turn facilitates F-actin coating *per se* and contributes to the protection of exocytic granule membranes, as discussed below.

Vacuole formation in acinar cells is thought to be an initial sign of acute pancreatitis in both animal models and the human disease (17, 18, 20). The present study has demonstrated, for the first time, that disruption of F-actin reorganization gives rise to such pathological vacuole formation, possibly as a result of destabilization of the Ω-profiles of exocytic granules and consequent granule swelling. Vacuole formation induced by high concentrations of CCK might be due to interference with the F-actin coating of granules by the sustained increase in $[Ca^{2+}]_i$ (19, 39), which may result in the activation of F-actin-severing proteins, such as gelsolin or villin, located in the apical region of the cell (22, 40, 41). Dismantling of F-actin coats may result from cleavage of the scaffolding protein plectin by caspage-8 (16). Our data further demonstrated that the increases in $[Ca^{2+}]_i$ were not sufficient for vacuole formation since large and sustained increases in $[Ca^{2+}]_i$ caused by photolysis of the caged-Ca^{2+} compound did not induce vacuole formation. CCK receptors are known to activate signaling cascades other than Ca^{2+} signaling (42). Such disruption of F-actin coating may account for the diffuse staining of F-actin detected previously in the pancreas of animal models of acute pancreatitis by one-photon confocal microscopy (16, 43).

Impairment of F-actin coating and consequent vacuole formation might explain the key features of the early phase of acute pancreatitis. First, aberrant activation of digestive enzymes has been detected within such vacuoles, possibly as a result of fusion of zymogen granules with lysosomes that contain cathepsin B (19, 20, 44, 45). The activation of digestive enzymes may be accelerated by vacuolar swelling, which results in enzyme retention. Indeed, inhibition of digestive enzyme secretion from the pancreas has been described in most experimental models of acute pancreatitis (20). Second, leakage of activated enzymes into the cytosol is thought to be a major contributing factor to acute pancreatitis (20). It is likely that the loss of F-actin coating results in the mechanical weakening of the granule membrane and thereby facilitates membrane rupture and leakage of activated enzymes into the cytosol. In addition, retention of activated digestive enzymes in vacuoles may induce the digestion of the vacuolar membrane and facilitate its rupture. Third, physiological acinar polarity is disrupted by vacuole formation (14, 44), which can result in granule fusion with the basolateral membrane (46, 47) and in the formation of basolateral protrusions (13), eventually leading to autodigestion of the pancreas.

In summary, two-photon excitation imaging has revealed that newly fused granules in pancreatic acinar cells are rapidly coated with F-actin. This coating of the granule membrane repairs the disruption of F-actin coating at the apical plasma membrane caused by exocytosis, thereby restoring the original rigidity of the apical membrane and preventing vacuole formation. Coating with F-actin only slows the rate of granule fusion, however; it does not reduce the overall extent of exocytosis. Thus, F-actin coating stabilizes structures generated by exocytosis and supports the physiological progression of this process. A similar regulatory mechanism based on actin polymerization may operate during membrane healing (48), which also involves compound exocytosis, in various cell types.

Acknowledgments—We thank T. Kise and N. Takahashi for technical assistance and S. Narumiya for exoenzyme C3.

REFERENCES

1. Etienne-Manneville, S., and Hall, A. (2002) *Nature* **420**, 629–635
2. Halpain, S. (2000) *Trends Neurosci.* **23**, 141–146
3. Reinhard, M., Jarchau, T., and Walter, U. (2001) *Trend. Biochem. Sci.* **26**, 243–249
4. Muallem, S., Kwiatkowska, K., Xu, X., and Yin, H. L. (1995) *J. Cell Biol.* **128**, 589–598
5. Orci, L., Gabbay, K. H., and Malaisse, W. J. (1972) *Science* **175**, 1128–1130
6. Trifaro, J. M., Rodriguez del Castillo, A., and Vitale, M. L. (1992) *Mol. Neurobiol.* **6**, 339–358
7. Valentijn, K., Valentijn, J. A., and Jamieson, J. D. (1999) *Biochem. Biophys. Res. Commun.* **266**, 652–661
8. Ichikawa, A. (1965) *J. Cell Biol.* **24**, 369–385
9. Palade, G. (1975) *Science* **189**, 347–358
10. Nemoto, T., Kimura, R., Ito, K., Tachikawa, A., Miyashita, Y., Iino, M., and Kasai, H. (2001) *Nat. Cell Biol.* **3**, 253–258
11. Schafer, C., Ross, S. E., Bragado, M. J., Groblewski, G. E., Ernst, S. A., and Williams, J. A. (1998) *J. Biol. Chem.* **273**, 24173–24180
12. Valentijn, J. A., Valentijn, K., Pastore, L. M., and Jamieson, J. D. (2000) *Proc. Natl. Acad. Sci. U. S. A.* **97**, 1091–1095
13. Burnham, D. B., and Williams, J. A. (1982) *Cell Tissue Res.* **222**, 201–212
14. O'Konski, M. S., and Pandol, S. J. (1990) *J. Clin. Invest.* **86**, 1649–1657
15. Jungermann, J., Lerch, M. M., Weidenbach, H., Lutz, M. P., Kruger, B., and Adler, G. (1995) *Am. J. Physiol.* **31**, G328–G338
16. Beil, M., Leser, J., Lutz, M. P., Gukovskaya, A., Seufferlein, T., Lynch, G., Pandol, S. J., and Adler, G. (2002) *Am. J. Physiol.* **282**, G450–G460
17. Kloppel, G. (1994) in *Acute Pancreatitis: Diagnosis and Therapy* (Bradley, E. L., III, ed) pp. 35–45, Raven, New York
18. Lampel, M., and Kern, H. F. (1977) *Virchows Arch. A Pathol. Anat. Histol.* **373**, 97–117
19. Raraty, M., Ward, J., Erdemli, G., Vaillant, C., Neoptolemos, J. P., Sutton, R., and Petersen, O. H. (2000) *Proc. Natl. Acad. Sci. U. S. A.* **97**, 13126–13131

20. Steer, M. L. (1999) *Baillieres Best Pract. Res. Clin. Gastroenterol.* **13,** 213–225
21. Denk, W., Strickler, J. H., and Webb, W. W. (1990) *Science* **248,** 73–76
22. Drenckhahn, D., and Mannherz, H. G. (1983) *Eur. J. Cell Biol.* **30,** 167–176
23. Torgerson, R. R., and McNiven, M. A. (2000) *J. Cell. Physiol.* **182,** 438–447
24. Hall, A. (1998) *Science* **279,** 509–514
25. Kasai, H., and Augustine, G. J. (1990) *Nature* **348,** 735–738
26. Coue, M., Brenner, S. L., Spector, I., and Korn, E. D. (1987) *FEBS Lett.* **213,** 316–318
27. Morii, N., and Narumiya, S. (1995) *Methods Enzymol.* **256,** 196–206
28. Cooper, J. A. (1987) *J. Cell Biol.* **105,** 1473–1478
29. Shin, D. M., Zhao, X.-S., Zeng, W., Mozhayeva, M., and Muallem, S. (2000) *J. Cell Biol.* **150,** 1101–1112
30. Ito, K., Miyashita, Y., and Kasai, H. (1997) *EMBO J.* **16,** 242–251
31. De Camilli, P., Peluchetti, D., and Meldolesi, J. (1976) *J. Cell Biol.* **70,** 59–74
32. Sahara, N., and Suzuki, K. (1990) *Cell Tissue Res.* **261,** 461–466
33. Hart, M. J., Jiang, X., Kozasa, T., Roscoe, W., Singer, W. D., Gilman, A. G., Sternweis, P. C., and Bollag, G. (1998) *Science* **280,** 2112–2114
34. Takai, Y., Sasaki, T., and Motozaki, T. (2001) *Physiol. Rev.* **81,** 152–208
35. Yin, H. L., and Janmey, P. A. (2003) *Annu. Rev. Physiol.* **65,** 761–789
36. Fuchs, E., and Yang, Y. (1999) *Cell* **98,** 547–550
37. Takahashi, N., Hatakeyama, H., Okado, H., Miwa, A., Kishimoto, T., Kojima, T., Abe, T., and Kasai, H. (2004) *J. Cell Biol.* **165,** 255–262
38. Sokac, A. M., Co, C., Taunton, J., and Bement, W. (2003) *Nat. Cell Biol.* **5,** 727–732
39. Ward, J. B., Petersen, O. H., Jenkins, S. A., and Sutton, R. (1995) *Lancet* **346,** 1016–1019
40. Janmey, P. A., and Matsudaira, P. T. (1988) *J. Biol. Chem.* **263,** 16738–16743
41. Bretscher, A., and Weber, K. (1980) *Cell* **20,** 839–847
42. Williams, J. A., Sans, M. D., Tashiro, M., Schafer, C., Bragado, M. J., and Dabrowski, A. (2002) *Pharmacol. Toxicol.* **91,** 297–303
43. Leser, J., Beil, M. F., Musa, O. A., Adler, G., and Lutz, M. P. (2000) *Am. J. Physiol.* **278,** G486–G491
44. Watanabe, O., Baccino, F. M., Steer, M. L., and Meldolesi, J. (1984) *Am. J. Physiol.* **246,** G457–G467
45. Kukor, Z., Mayerle, J., Kruger, B., Toth, M., Steed, P. M., Halangk, W., Lerch, M. M., and Sahin-Toth, M. (2002) *J. Biol. Chem.* **277,** 21389–21396
46. Scheele, G., Adler, G., and Kern, H. (1987) *Gastroenterology* **92,** 345–353
47. Gaisano, H. Y., Lutz, M. P., Leser, J., Sheu, L., Lynch, G., Tang, L., Tamori, Y., Trimble, W. S., and Salapatek, A. M. F. (2001) *J. Clin. Invest.* **108,** 1597–1611
48. Miyake, K., McNeil, P. L., Suzuki, K., Tsunoda, R., and Sugai, N. (2001) *J. Cell Sci.* **114,** 3487–3494
49. Takahashi, N., Kishimoto, T., Nemoto, T., Kadowaki, T., and Kasai, H. (2002) *Science* **297,** 1349–1352

Eur Arch Psychiatry Clin Neurosci (2004) 254 : 245–251 DOI 10.1007/s00406-004-0488-z

ORIGINAL PAPER

Shuji Asahi · Yasumasa Okamoto · Go Okada · Shigeto Yamawaki · Norio Yokota

Negative correlation between right prefrontal activity during response inhibition and impulsiveness: A fMRI study

Received: 5 May 2003 / Accepted: 8 December 2003

Abstract Behavioral disinhibition in Go/No-Go task is thought to be associated with impulsiveness in humans. Recent imaging studies showed that neural circuits involving diverse areas of the frontal cortex and other association cortex sites such as the parietal cortex are implicated in the inhibition of response during No-Go trials. The aim of the present study was to investigate the association between regional cerebral activation during No-Go trials and impulsiveness. Seventeen right-handed healthy volunteers participated in the study. We used functional magnetic resonance imaging to measure the brain activation during a Go/No-Go task. The Barratt Impulsiveness Scale, 11th version (BIS-11) was used to measure impulsiveness. Activated regions included the right middle frontal gyrus and the inferior parietal lobe, which is consistent with previous neuroimaging studies. A negative correlation was observed between the motor impulsiveness of BIS-11 and No-Go-related activation in the right dorsolateral prefrontal cortex (RDLPFC). Our results suggest that the RDLPFC is the area most sensitive to differences in individual motor impulsiveness and its activity may be an indicator of the individual capacity for response inhibition.

Key words response inhibition · fMRI · right dorsolateral prefrontal cortex (RDLPFC) · impulsiveness · BIS

Sh. Asahi · Y. Okamoto · G. Okada · Sh. Yamawaki, M.D., Ph.D. (✉)
Department of Psychiatry and Neurosciences
Graduate School of Biomedical Sciences
Hiroshima University
1-2-3 Kasumi, Minami-ku
Hiroshima, 734-8551, Japan
Tel.: +81-82/257-5205
Fax: +81-82/257-5209
E-Mail: yamawaki@hiroshima-u.ac.jp

N. Yokota
Hiroshima Prefectural College of Health and Welfare
Hiroshima, 723-0053, Japan

Introduction

Impulsiveness is a dimensional personality trait that is important for a wide range of different human behaviors. Although a strict definition of impulsiveness is difficult to establish, biological, psychological and social studies have regarded impulsiveness as 'a predisposition toward rapid, unplanned reactions to internal or external stimuli without regard to the negative consequences of these reactions to the impulsive individual or to others' [34]. Recent laboratory investigations of impulsiveness showed two dominant models: (1) *Reward-delay impulsivity*, which is the inability to delay reward and leads to an increased tendency to choose immediate small rewards over larger delayed ones [35]; and (2) *Rapid-response impulsivity*, which is the inability to conform responses to environmental context and leads to errors of commission on tests that require careful checking of stimuli [16]. The latter model appeared to be more closely related to trait impulsiveness, which was measured by the Barratt Impulsiveness Scale (BIS), a popular self-reporting impulsiveness scale [37], and was increased in subjects with a lifetime Axis I or Axis II diagnosis [49].

The ability to inhibit behavioral responses that are inappropriate in the current context is a response inhibition essential for normal behavior, and is thought to be associated with *Rapid-response impulsivity* in humans. This inhibitory function has been investigated frequently using the Go/No-Go task, in which the participants are required to refrain from responding to designated items within a series of stimuli. The prefrontal cortex (PFC) has been implicated in behavioral inhibition, based on animal, clinical and neuroimaging studies. Studies in monkeys demonstrated that lesions in the PFC resulted in difficulties in behavioral inhibition [8, 24, 45], as well as the studies of patients with lesions in the same region [22]. Recent neuroimaging studies using PET or fMRI have shown a right hemispheric dominance of inhibitory control that involves diverse areas of

the frontal cortex and other association cortex sites, such as the parietal cortex, which are implicated in response inhibition during No-Go trials [21, 26, 30]. Although human impulsiveness was revealed to associate with some biological markers [1, 17, 42, 50], the region of the brain that is directly correlated with human impulsiveness is still unclear.

Some experiments used only behavioral laboratory measurements of impulsiveness [11, 21], which do not incorporate the cognitive or social aspects of impulsiveness and do not measure long-term patterns of behavior. This may explain the inconsistency in the findings of those previous studies [9, 33, 38]. Another way to examine impulsiveness is to use self-reporting measurements such as BIS, which has the advantage of generating information on a variety of types of acts and on whether these acts continue as long-term patterns of behavior. In general, a closer association and a greater consistency has been demonstrated among different self-report impulsiveness scales [3, 9, 15].

The aim of the present study was to clarify the brain areas associated with impulsiveness, as measured by BIS-11. Based on the studies cited above, we hypothesized that the degree of activation in some areas within the right hemispheric dominance of neural networks was correlated with the degree of impulsiveness.

Methods

Subjects

Seventeen right-handed healthy volunteers (10 men and 7 women), aged 23–30 years (mean: 25.1 years), and with no history of neurological or psychiatric illness, participated in the study. Handedness was assessed by the Edinburgh Handedness Inventory [36]. The subjects were recruited from the Kansai area in Japan and were paid ¥7,000 for their participation in the study. The study was conducted under a protocol that was approved by the Ethics Committee of Hiroshima University School of Medicine. All subjects submitted informed written consent of their participation.

Barratt Impulsiveness Scale, 11th version

The BIS-11 [37], a short questionnaire designed to measure impulsiveness, has been validated in impulsive and normal populations. The questionnaire contains a total of 30 items, each of which is answered on a 4-point Likert scale (rarely/never = 1, occasionally = 2, often = 3, almost always/always = 4), and the level of impulsiveness is calculated by summing up the scores for each item. All items are defined as identifying impulsiveness within the structure of related personality traits and are divided into three subscales: attention (inattention and cognitive instability), motor (motor impulsiveness and lack of perseverance), and non-planning (lack of self-control and intolerance of cognitive complexity). The Japanese version of the BIS-11 was developed using a back-translation method and was judged to be a reliable and valid measure in the Japanese population [47]. Subjects completed the BIS-11 after the task procedure.

Experimental tasks

The task consisted of eight alternating 36-s epochs of Go and No-Go conditions. During the experiment, subjects viewed a series of letters once every 1500 ms and responded with a key press to every letter except the letter 'X', to which they were instructed to withhold response. All subjects responded using the forefinger of the right hand. Stimulus duration was 500 ms and the interstimulus interval was 1000 ms for both conditions. Subjects were instructed to try to respond while the stimulus was on the screen. In the Go (control) condition, subjects were presented a random sequence of letters other than the letter 'X'. In the No-Go condition, subjects were presented with the letter 'X' 50% of the time, thus requiring a response to half the trials (Go trials) and a response inhibition to the other half (No-Go trials). The high frequency of targets was maintained across the entire experiment, which generated a compelling tendency to respond. In order to ensure correct performance, the subjects were trained outside the task scanner until they understood the task completely. Motor responses were made using a fiber-optic response pad (Current Designs Inc, Philadelphia). The task consisted of eight blocks, each of which continues without being preceded by an instruction. The subjects could not distinguish the boundary between the conditions; therefore, different strategies are not imposed on the subject for the different conditions.

fMRI acquisition

Functional magnetic resonance imaging (fMRI) was performed using a Magnex Eclipse 1.5T Power Drive 250 (Marconi Medical Systems, USA). A time-course series of 107 volumes was acquired with T2*-weighted, gradient echo, echo planar imaging (EPI) sequences. Each volume consisted of 38 slices, and the slice thickness was 4.0 mm with no gap to cover the entire cerebral and cerebella cortex. The interval between two successive acquisitions of the same image (TR) was 4000 ms, echo time (TE) was 55 ms, and the flip angle was 90°. The field of view was 256 mm, and the matrix size was 64 × 64, giving voxel dimensions of 4.0 × 4.0 × 4.0 mm. After functional scanning, structural scans were acquired using Tl-weighted gradient echo pulse sequence (TR = 12 ms; TE = 4.5 ms; Flip angle = 20°; FOV = 256 mm; voxel dimensions of 1.0 × 1.0 × 1.0 mm), which facilitated the localization and coregistration of functional data.

Analysis

The image data were analyzed by statistical parametric mapping (SPM99 software from the Wellcome Department of Cognitive Neurology, London, UK) implemented in Matlab (Mathworks Inc., Sherborn, MA). The first three volumes of each fMRI run (prescan period) were discarded because the magnetization was unsteady. The remaining 104 volumes were used for the statistical analysis. Images were corrected for motion and realigned, using the first scan of the session as a reference. T1 anatomical images were coregistered to the first functional scans and aligned to the T1 template included in SPM99. The calculated nonlinear transformation was applied to all functional images for spatial normalization. Finally, the functional images were smoothed with an 8 mm full-width, half-maximum (FWHM) Gaussian filter. Using group analysis according to a random effect model [18], we identified regions that showed significant responses to the No-Go condition compared with that of the Go condition as areas related to response inhibition. The group analysis consisted of two levels. In the first level, the signal time course of each subject was modeled with a delayed box-car function convolved with a hemodynamic response function in the context of a general linear model. One contrast image per subject was created by contrasting the No-Go conditions with the Go conditions. These images were entered into a one-sample t-test, which allowed us to identify regions of the brain that were significantly activated by the response inhibition function during the No-Go condition as compared to the Go condition. The resulting foci were then characterized in terms of spatial extent (k) and peak height (u). The significance of each region was estimated using distribution approximations from the theory of Gaussian fields. This characterization is in terms of the probability that a region of the observed number of voxels (or greater) could have occurred by chance (extent threshold) over the entire volume analyzed. After locating and analyzing areas of the brain that showed sig-

nificant activation during the No-Go condition, we then performed a regression analysis on these areas only, to determine the association between the magnitude of brain activation in each area and the scores of the BIS-11. Activations were reported if they exceeded $p < 0.001$ (uncorrected) on the single voxel level and $p < 0.05$ (corrected) on the cluster level. In regression analysis, we masked with the regions that showed significant responses to the No-Go condition compared with that of the Go condition, as the areas related to response inhibition described above, to avoid identifying regions that were not activated for the No-Go condition compared with the Go condition. However, when using a lower threshold, an activation that was at a lower level but consistent with the significant activation noted above was seen over more widespread areas of the brain. This occurred because the threshold for this mask was set at $p < 0.05$ and larger areas are included in the final analysis of the response inhibition data. Therefore, significance was considered at a threshold of $p < 0.001$ and an extent of > 40 contiguous voxels. Labels for brain activation foci were obtained in Talairach coordinates using the Talairach Demon software, which provides an accuracy similar to that of neuroanatomical experts [28].

Behavioral analysis

Errors of commission (response to 'X') and omission (not to response to targets) were recorded, and the average response times to targets were calculated for each subject.

Results

Behavioral and BIS-11 results

Subjects performed well on the task, making a few commission errors (7.3%) and a few omission errors (1.3%). The response times to targets averaged 325.8 ± 20.8 ms. Average scores of the total BIS-11, attention-key, motor-key and non-planning-key were 68.9 ± 11.0, 19.7 ± 3.3, 21.1 ± 4.1 and 28.1 ± 5.3, respectively. Some correlation was detected among the BIS-11 scales. The total score of BIS-11 was strongly correlated with all of the 3 subscales (attention-key: $r = 0.69$, $p < 0.01$; motor-key: $r = 0.89$, $p < 0.01$; non-planning-key: $r = 0.93$, $p < 0.01$). Among the subscales, the non-planning-key and attention-key ($r = 0.51$, $p < 0.05$), or non-planning-key and motor-key ($r = 0.79$, $p < 0.01$) were correlated. There was also a trend between attention-key and motor-key, though not significant ($r = 0.48$, $p = 0.05$). These results were natural because the BIS-11 has sufficient internal consistency reliability [47]. No correlation was observed between the performance data (i. e., number of commission errors or omission errors, average response time to targets) and the BIS-11 scores.

fMRI data

For fMRI data analysis, the threshold for activation was set at $p < 0.001$ for voxel level. In Fig. 1 and Table 1, the activation, which was corrected for multiple comparisons at the extent threshold of $p < 0.05$, is shown. Four independent areas of activation, which were predominantly right-lateralized, were observed to underlie response inhibition. These areas, including the Talairach coordinates of their centers-of-mass, are presented in Table 1. The No-Go condition, in comparison to the Go condition, resulted in the significant activation of the right middle and superior temporal gyrus, the right precentral gyrus, the right middle frontal gyrus, and the right cuneus and precuneus.

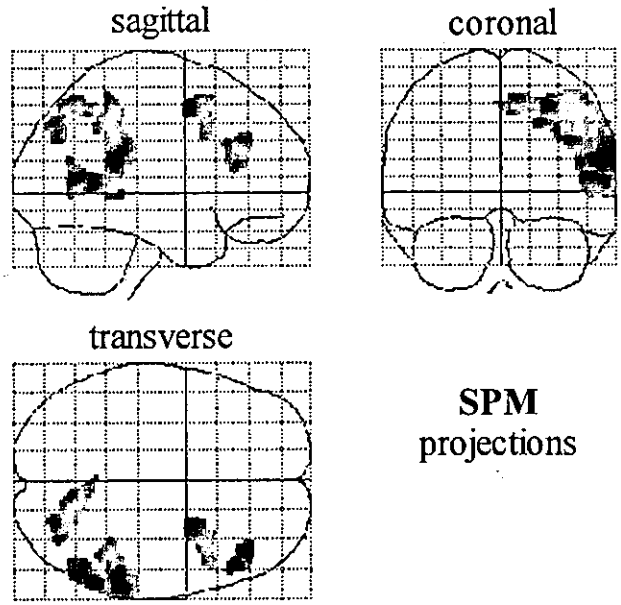

Fig. 1 Statistical parametric maps of brain regions (on the second level group analysis for the 17 subjects) showing significant activation associated with the NO-GO condition, compared with the GO condition at a statistical threshold of $P < 0.001$ (uncorrected) on the single voxel level and $P < 0.05$ (corrected) on the cluster level. For exact coordinates, see Table1. Clusters of activation are shown as through-projections onto representations of standard stereotactic space. *Sagittal* side view; *coronal* view from back; *transverse* view from above

Regression analysis revealed a significant negative correlation between the motor-key score of BIS-11 and the magnitude of brain activation during response inhibition in the right middle frontal gyrus (x, y, z = 34, 22, 29; area 9; t-value = 5.66; 42 voxels; $r = -0.93$; $p < 0.01$) showed in Fig. 2A, B. Other BIS-11 scores (i. e., total BIS-11, attention-key and non-planning-key) did not show a significant association with the magnitude of brain activation during response inhibition. Furthermore, no significant correlation was observed between the performance data (i. e., the number of commission errors and omission errors, response time) and the magnitude of brain activation during response inhibition.

By analyzing the mean percentage signal changes in the regions shown in Fig. 1 and Table 1, we sought to find the possible functional connectivity among the regions concerning response inhibition. Consequently, we detected a correlation between the areas including the right middle frontal/the right precentral gyrus and the right cuneus/precuneus ($r = 0.65$, $p < 0.01$). There was no correlation between the other regions.

Table 1 Brain areas significantly activated during response inhibition

Area	BA	Cluster level p	Cluster level k	Voxel level p	Voxel level T	x	y	z
R superior temporal gyrus	22	0.000	1193	0.003	9.82	58	−42	18
R middle temporal gyrus	37			0.095	7.05	60	−52	8
R middle temporal gyrus	37			0.153	6.67	52	−60	10
R middle frontal gyrus	6	0.003	276	0.133	6.78	26	4	50
R precentral gyrus	9			0.983	4.42	44	12	38
R middle frontal gyrus	9	0.005	258	0.177	6.55	40	34	30
R middle frontal gyrus	46			0.288	6.15	48	30	18
R middle frontal gyrus	46			0.639	5.38	52	26	26
R cuneus	7	0.001	332	0.230	6.34	24	−76	40
R cuneus	19			0.292	6.14	34	−74	34
R precuneus	7			0.596	5.46	10	−66	52

The names of areas described above point to the peaks of activation within each cluster
p corrected p values for spatial extent (cluster level p value) and peak height (voxel level p value) of the activation: all areas exceeding the corrected cluster level threshold of 0.05 are displayed; *k* number of voxels in cluster; *T* t score; *x, y, z* localization according to the standard Talairach coordinates (in mm); *L* left; *R* right

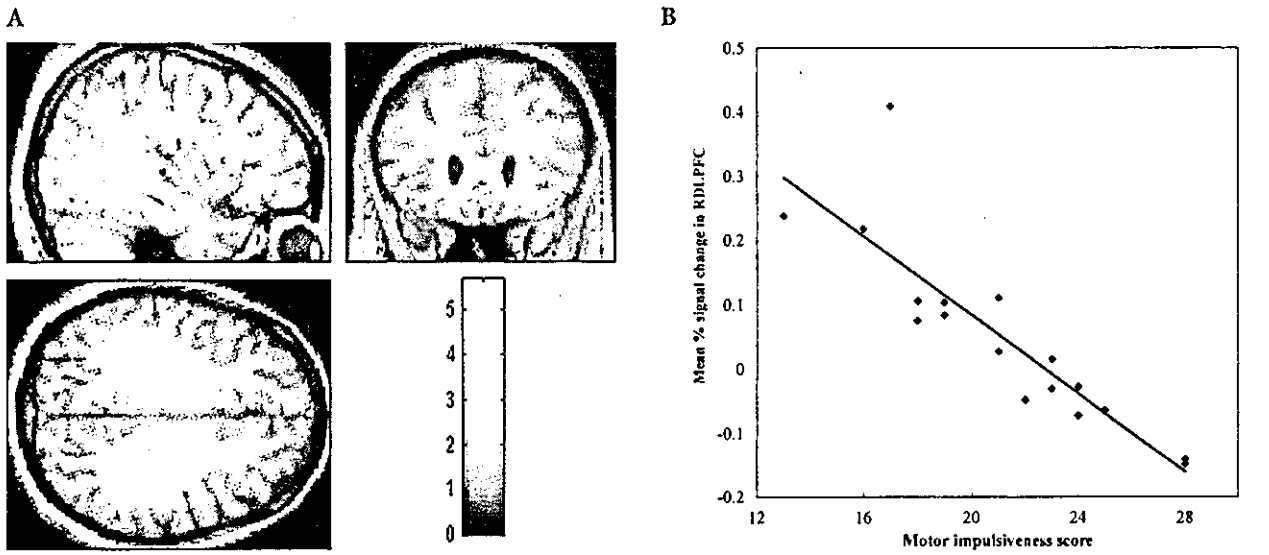

Fig. 2 **A** Statistical parametric maps of brain region (on the regression analysis for the 17 subjects) showing significant activation negatively associated with the motor-key score of BIS-11, within the areas activated during response inhibition, at a statistical threshold of $P < 0.05$ (uncorrected) on the single voxel level and $P < 0.05$ (corrected) on the cluster level. The region corresponds to the RDLPFC: x, y, z = 34, 22, 29; area 9; t-value = 5.66; 42 voxels. Clusters of activation are shown as through-projections onto representations of standard stereotactic space. *Sagittal* side view; *coronal* view from back; *transverse* view from above. **B** Correlation between mean percentage of signal change within the RDLPFC shown in Fig. 2A and the motor-key scores of BIS-11. The correlation coefficient is $r = -0.93$; $p < 0.01$

Discussion

In the present study, we examined the brain areas associated with impulsiveness as measured by BIS-11 in healthy volunteers. We have shown a significant negative correlation between the motor-key score of BIS-11 and the magnitude of activation in the right dorsolateral prefrontal cortex (RDLPFC) during the No-Go condition compared to that of the Go condition (i. e., as the motor-key score of BIS-11 increases, the signal intensity seen in the region including the RDLPFC decreases). These results suggest that the RDLPFC may play a more important role in response inhibition in motor inhibitory control than other brain regions.

We used BIS-11, a self-report measure, in the assessment of impulsiveness. This scale was designed to measure temperament, a long lasting characteristic of the personality of the subject. In addition, we can gather consistent information that is not affected by experimental methods or tasks. Our results illuminated the motor impulsiveness of BIS-11 as only a subscale, which has a significant association with the activation in the RDLPFC during response inhibition. Although the BIS-11 and its subscales have sufficient internal consistency reliability, other subscales did not show any association

between any brain regions activated during response inhibition. That may be because the Go/No-Go task we employed is a task emphasized on the motor response inhibition. Barratt (1994) reported that college students scored higher on average for motor impulsiveness than a mixed adult population and lower for cognitive impulsiveness, whereas a group of psychiatric inpatients scored high mainly on the non-planning impulsiveness [2]. This indicates that motor impulsiveness is more sensitive than other subscales of BIS (i. e. cognitive impulsiveness and non-planning impulsiveness) in young healthy persons and supports our result, which illuminated motor impulsiveness in our comparatively young (25.1 years old on average) healthy subjects.

In this study, brain activation associated with successful response inhibition was observed as a distributed network in the right hemisphere, which was consistent with the results of previous functional brain imaging studies that suggest right hemisphere regions, including the RDLPFC, the inferior parietal cortex and, medially, the anterior cingulate cortex (ACC), are especially important for inhibitory control [6, 7, 13, 20, 21, 27, 43]. In particular, the importance of the RDLPFC was emphasized after regression analysis. The RDLPFC is one of the most consistently activated areas in regard to inhibitory control, and is thought to participate in the active suppression of inappropriate movement and behavior. The right lateral prefrontal regions have been shown to be activated in countering proactive interference [7], set-shifting involving the inhibition of the previous rule in the Wisconsin Card Sorting task [27], response inhibition in the Stop paradigm [39, 43], suppression of imitative behavior [5], and a range of clinical disinhibition syndromes that follow right hemisphere damage [46, 48]. In addition to being involved in the suppression of movement and behavior, the RDLPFC is also associated with the voluntary suppression of a positive emotional reaction, such as sexual arousal [4], and the voluntary suppression of a negative emotion, such as sadness [29]. These facts indicate that the RDLPFC is a key structure involved in the variety of inhibitory control.

We did not observe any significant correlation between the performance data (i. e., the number of commission errors and omission errors, response time) and the magnitude of brain activation during response inhibition. This result is not consistent with the results of Garavan et al. (1999), which suggest that the faster a subject was in responding to the targets, the greater the signal intensity seen in the regions, including the right inferior frontal cluster and the left inferior parietal lobule cluster, during response inhibition [21]. Comparing our performance data with theirs, the percentage of commission errors and omission errors are almost the same. Therefore, it may be difficult to interpret the inconsistency simply as the task level of difficulty. Another possible interpretation is the difference of strategies in executing the task. The response time to targets and the accuracy of responses are conflicting natures in executing the Go/No-Go task. Both of these parameters may be sensitive and variable to the difference in strategies each subject used to emphasize the response time to targets or the accuracy of responses, when they are demanded to manage both. Actually, the mean response time to targets in our subjects (326 ms) was considerably shorter than that of the subjects in the other study (460 ms).

Casey et al. (1997) showed a significant negative correlation between the number of commission errors and the volume of activation in the orbital frontal gyrus [11]. Regrettably, our experimental conditions did not show a significant activation in the orbitofrontal cortex, as did other fMRI studies. This inconsistency may be due to the difference of methods employed. The correlation the other studies observed maybe reflected the developmental difference between adults and children, because those studies mixed adults and children as subjects in their experiment. In fact, those studies also showed that the volume of activation was significantly greater in children relative to adults when performing the No-Go condition of the task. However, the location of activation in the PFC was not different between the age groups. This observation may be due to susceptibility effects at the air-tissue interface in the perinasal sinuses, which renders orbitofrontal activation difficult to observe in fMRI. However, lesion studies in animals and in humans have traditionally implicated the orbitofrontal cortex in behavioral inhibition [19]. Therefore, we cannot exclude a potential role of the orbitofrontal cortex in inhibitory control based on fMRI data.

Liddle et al. (2001) [30] reported that the activation of ACC during No-Go trials was not substantially greater than that during Go trials under circumstances in which No-Go trials and Go trials were equally probable. In addition, they reported that the activation of ACC was related to decision formation and monitoring, rather than to response inhibition. These results may explain why our results have not shown activation in the ACC. We used a standard blocked design [11] in this study as a way to provide and maintain a high level of prepotent response. Randomly presenting an equal number of Go and No-Go stimuli would have eliminated a buildup of a prepotent response. In such a situation, the subjects were required to make and monitor decisions attentively during both conditions, which might result in little difference between the activation of the ACC during No-Go conditions and that during Go conditions.

In addition to those areas discussed above, we detected activities in other areas including the right middle frontal/the right precentral gyrus (frontal cortex) and the right cuneus/precuneus (parietal cortex). Moreover, a correlation was detected between both areas by analyzing the mean percentage signal changes in the regions during response inhibition. The observed activation in these two areas might be related to motor imagery, which is defined as the mental simulation of a motor act [12, 14], and is reported from neuroimaging studies to share neural substrates with those underlying motor execution [31, 40, 41]. The precentral sulcus at the level of middle

frontal gyrus and the posterior superior parietal/precuneus were reported to be activated more during motor imagery than the motor execution [23] and are thought to correspond to a 'negative motor area' where electrical stimulation causes a cessation of movement [32] because activity for inhibiting movement would be needed during motor imagery. Therefore, our observation that these areas are activated may be reasonable.

One of the most important issues of the present results is why high impulsive subjects perform as well as low impulsive subjects with less activity in the RDLPFC. It may be possible to explain this by the fact that a parametric manipulation of the ratio between Go and No-Go stimuli revealed the RDLPFC increases as inhibitory difficulty decreased, that is, as the relative numbers of No-Go stimuli increased, thereby diminishing response prepotency [10, 13]. That is thought to reflect the importance of maintaining relevant stimulus information against interference from competing non-target stimuli. Therefore, the high impulsive subjects with less activation in the RDLPFC may have less capacity left for response inhibition than that of less impulsive subjects. However, some fMRI studies concerning working memory showed an increased activity in the PFC with increasing memory loads, possibly due to a limited capacity of the system for controlled processing [25, 44]. Therefore, the relationship between the task difficulty and the activation in the PFC may depend on the tasks which require different processes of cognitive functions. Further studies are needed to clarify this issue.

One of the limitations of this study is that a block design was used for investigating motor response suppression. When employing block design, it is difficult to control for the difference in frequency of motor responses between blocks that differ in the proportion of Go and No-Go events. Casey et al. (1997) tried to avoid this difficulty by comparing the epochs containing Go and No-Go responses with two baseline conditions that contained only Go trials. One baseline was established from a frequency of Go trials that matched that in the No-Go condition (ensuring approximate matching of number of motor responses), while the other baseline was established with the total number of trials matching the No-Go condition (ensuring matching of the number of stimuli presented) [11]. Their results showed that the same areas were activated during No-Go conditions and Go conditions in both contrasts. Together, these results may support the validity of our study using the latter baseline. Another possible limitation is in measuring impulsiveness using questionnaires, which are subjective. Shortcomings on self-report measures include the need to rely on the honesty of the individuals completing the questionnaire.

Conclusion

We observed a negative correlation between the motor impulsiveness assessed by BIS-11 and the activation of the RDLPFC during response inhibition in healthy subjects. Our findings highlight the importance of the activity in the RDLPFC as the area most sensitive to the differences in individual motor impulsiveness, even in the healthy subjects. However, the role of the RDLPFC remains unclear, thus, further studies are needed.

References

1. af Klinteberg B, Schalling D, Edman G, Oreland L, Asberg M (1987) Personality correlates of platelet monoamine oxidase (MAO) activity in female and male subjects. Neuropsychobiology 18:89–96
2. Barratt ES (1994) Impulsiveness and aggression. In: Monahan J, Steadman HJ (eds) Violence and mental disorder: developments in risk assessment, Chicago. University of Chicago Press, pp 61–79
3. Barratt ES (1985) Impulsiveness subtraits, arousal and information processing. In: Spence JT, Itard CE (eds) Motivation, emotion and personality. North Holland: Elsevier Science, pp 137–146
4. Beauregard M, Levesque J, Bourgouin P (2001) Neural correlates of conscious self-regulation of emotion. J Neurosci 21:RC165
5. Brass M, Zysset S, von Cramon DY (2001) The inhibition of imitative response tendencies. Neuroimage 14:1416–1423
6. Braver TS, Barch DM, Gray JR, Molfese DL, Snyder A (2001) Anterior cingulate cortex and response conflict: effects of frequency, inhibition and errors. Cereb Cortex 11:825–836
7. Bunge SA, Ochsner KN, Desmond JE, Glover GH, Gabrieli JD (2001) Prefrontal regions involved in keeping information in and out of mind. Brain 124:2074–2086
8. Butters N, Butter C, Rosen J, Stein D (1973) Behavioral effects of sequential and one-stage ablations of orbital prefrontal cortex in the monkey. Exp Neurol 39:204–214
9. Carrillo-de-la-Pena MT, Otero JM, Romero E (1993) Comparison among various methods of assessment of impulsiveness. Percept Mot Skills 77:567–575
10. Casey BJ, Forman SD, Franzen P, Berkowitz A, Braver TS, Nystrom LE, Thomas KM, Noll DC (2001) Sensitivity of prefrontal cortex to changes in target probability: a functional MRI study. Hum Brain Mapp 13:26–33
11. Casey BJ, Trainor RJ, Orendi JL, Schubert AB, Nystrom LE, Giedd JN, Castellanos FX, Haxby JV, Noll DC, Cohen JD, Forman SD, Dahl RE, Rapoport JL (1997) A developmental functional MRI study of prefrontal activation during performance of a go/no-go task. J Cogn Neurol 9:835–847
12. Crammond DJ (1997) Motor imagery: never in your wildest dream. Trends Neurosci 20:54–57
13. de Zubicaray GI, Andrew C, Zelaya FO, Williams SC, Dumanoir C (2000) Motor response suppression and the prepotent tendency to respond: a parametric fMRI study. Neuropsychologia 38: 1280–1291
14. Decety J (1996) The neurophysiological basis of motor imagery. Behav Brain Res 77:45–52
15. Dickman SJ (1990) Functional and dysfunctional impulsivity: personality and cognitive correlates. J Pers Soc Psychol 58: 95–102
16. Evenden JL (1998) The pharmacology of impulsive behaviour in rats IV: the effects of selective serotonergic agents on a paced fixed consecutive number schedule. Psychopharmacology (Berl) 140:319–330
17. Fallgatter AJ, Herrmann MJ (2001) Electrophysiological assessment of impulsive behavior in healthy subjects. Neuropsychologia 39:328–333
18. Friston KJ, Holmes AP, Worsley KJ, (1999) How many subjects constitute a study? Neuroimage 10:1–5
19. Fuster JM (1989) The prefrontal cortex: Anatomy, Physiology and Neuropsychology of the Frontal Lobe. Raven Press, New York, p 110

20. Garavan H, Ross TJ, Murphy K, Roche RA, Stein EA (2002) Dissociable executive functions in the dynamic control of behavior: inhibition, error detection, and correction. Neuroimage 17: 1820–1829
21. Garavan H, Ross TJ, Stein EA (1999) Right hemispheric dominance of inhibitory control: an event-related functional MRI study. Proc Natl Acad Sci USA 96:8301–8306
22. Godefroy O, Rousseaux M (1996) Divided and focused attention in patients with lesion of the prefrontal cortex. Brain Cogn 30: 155–174
23. Hanakawa T, Immisch I, Toma K, Dimyan MA, Van Gelderen P, Hallett M (2003) Functional properties of brain areas associated with motor execution and imagery. J Neurophysiol 89:989–1002
24. Iversen SD, Mishkin M (1970) Perseverative interference in monkeys following selective loss of the inferior prefrontal convexity. Exp Brain Res 11:376–386
25. Jaeggi SM, Seewer R, Nirkko AC, Eckstein D, Schroth G, Groner R, Gutbrod K (2003) Does excessive memory load attenuate activation in the prefrontal cortex? Load-dependent processing in single and dual tasks: functional magnetic resonance imaging study. Neuroimage 19:210–225
26. Kawashima R, Satoh K, Itoh H, Ono S, Furumoto S, Gotoh R, Koyama M, Yoshioka S, Takahashi T, Takahashi K, Yanagisawa T, Fukuda H (1996) Functional anatomy of GO/NO-GO discrimination and response selection – A PET study in man. Brain Research 728:79–89
27. Konishi S, Nakajima K, Uchida I, Kikyo H, Kameyama M, Miyashita Y (1999) Common inhibitory mechanism in human inferior prefrontal cortex revealed by event-related functional MRI. Brain 122:981–991
28. Lancaster JL, Woldorff MG, Parsons LM, Liotti M, Freitas CS, Rainey L, Kochunov PV, Nickerson D, Mikiten SA, Fox PT (2000) Automated Talairach atlas labels for functional brain mapping. Hum Brain Mapp 10:120–131
29. Levesque J, Eugene F, Joanette Y, Paquette V, Mensour B, Beaudoin G, Leroux JM, Bourgouin P, Beauregard M (2003) Neural circuitry underlying voluntary suppression of sadness. Biol Psychiatry 53:502–510
30. Liddle PF, Kiehl KA, Smith AM (2001) Event-related fMRI study of response inhibition. Hum Brain Mapp 12:100–109
31. Lotze M, Montoya P, Erb M, Hulsmann E, Flor H, Klose U, Birbaumer N, Grodd W (1999) Activation of cortical and cerebellar motor areas during executed and imagined hand movements: an fMRI study. J Cogn Neurosci 11:491–501
32. Luders HO, Dinner DS, Morris HH, Wyllie E, Comair YG (1995) Cortical electrical stimulation in humans. The negative motor areas. Adv Neurol 67:115–129
33. Milich R, Kramer J (1984) Reflections on impulsivity: an empirical investigation of impulsivity as a construct. Advances in Learning and Behavioral Disabilities 3:57–94
34. Moeller FG, Barratt ES, Dougherty DM, Schmitz JM, Swann AC (2001) Psychiatric aspects of impulsivity. Am J Psychiatry 158: 1783–1793
35. Monterosso J, Ainslie G (1999) Beyond discounting: possible experimental models of impulse control. Psychopharmacology (Berl) 146:339–347
36. Oldfield RC (1971) The assessment and analysis of handedness: the Edinburgh inventory. Neuropsychologia 9:97–113
37. Patton JH, Stanford MS, Barratt ES (1995) Factor structure of the Barratt impulsiveness scale. J Clin Psychol 51:768–774
38. Paulsen K, Johnson M (1980) Impulsivity: a multidimensional concept with developmental aspects. J Abnorm Child Psychol 8: 269–277
39. Pliszka SR, Liotti M, Woldorff MG (2000) Inhibitory control in children with attention-deficit/hyperactivity disorder: event-related potentials identify the processing component and timing of an impaired right-frontal response-inhibition mechanism. Biol Psychiatry 48:238–246
40. Porro CA, Cettolo V, Francescato MP, Baraldi P (2000) Ipsilateral involvement of primary motor cortex during motor imagery. Eur J Neurosci 12:3059–3063
41. Porro CA, Francescato MP, Cettolo V, Diamond ME, Baraldi P, Zuiani C, Bazzocchi M, di Prampero PE (1996) Primary motor and sensory cortex activation during motor performance and motor imagery: a functional magnetic resonance imaging study. J Neurosci 16:7688–7698
42. Reist C, Helmeste D, Albers L, Chhay H, Tang SW (1996) Serotonin indices and impulsivity in normal volunteers. Psychiatry Res 60:177–184
43. Rubia K, Russell T, Overmeyer S, Brammer MJ, Bullmore ET, Sharma T, Simmons A, Williams SC, Giampietro V, Andrew CM, Taylor E (2001) Mapping motor inhibition: conjunctive brain activations across different versions of go/no-go and stop tasks. Neuroimage 13:250–261
44. Rypma B, Berger JS, D'Esposito M (2002) The influence of working-memory demand and subject performance on prefrontal cortical activity. J Cogn Neurosci 14:721–731
45. Sasaki K, Gemba H, Tsujimoto T (1989) Suppression of visually initiated hand movement by stimulation of the prefrontal cortex in the monkey. Brain Res 495:100–107
46. Shulman KI (1997) Disinhibition syndromes, secondary mania and bipolar disorder in old age. J Affect Disord 46:175–182
47. Someya T, Sakado K, Seki T, Kojima M, Reist C, Tang SW, Takahashi S (2001) The Japanese version of the Barratt Impulsiveness Scale, 11th version (BIS-11): its reliability and validity. Psychiatry Clin Neurosci 55:111–114
48. Starkstein SE, Robinson RG (1997) Mechanism of disinhibition after brain lesions. J Nerv Ment Dis 185:108–114
49. Swann AC, Bjork JM, Moeller FG, Dougherty DM (2002) Two models of impulsivity: relationship to personality traits and psychopathology. Biol Psychiatry 51:988–994
50. Walderhaug E, Lunde H, Nordvik JE, Landro NI, Refsum H, Magnusson A (2002) Lowering of serotonin by rapid tryptophan depletion increases impulsiveness in normal individuals. Psychopharmacology (Berl) 164:385–391

nature neuroscience

Prediction of immediate and future rewards differentially recruits cortico-basal ganglia loops

Saori C Tanaka[1–3], Kenji Doya[1–3], Go Okada[3,4], Kazutaka Ueda[3,4], Yasumasa Okamoto[3,4] & Shigeto Yamawaki[3,4]

Evaluation of both immediate and future outcomes of one's actions is a critical requirement for intelligent behavior. Using functional magnetic resonance imaging (fMRI), we investigated brain mechanisms for reward prediction at different time scales in a Markov decision task. When human subjects learned actions on the basis of immediate rewards, significant activity was seen in the lateral orbitofrontal cortex and the striatum. When subjects learned to act in order to obtain large future rewards while incurring small immediate losses, the dorsolateral prefrontal cortex, inferior parietal cortex, dorsal raphe nucleus and cerebellum were also activated. Computational model–based regression analysis using the predicted future rewards and prediction errors estimated from subjects' performance data revealed graded maps of time scale within the insula and the striatum: ventroanterior regions were involved in predicting immediate rewards and dorsoposterior regions were involved in predicting future rewards. These results suggest differential involvement of the cortico-basal ganglia loops in reward prediction at different time scales.

In daily life, people make decisions based on the prediction of rewards at different time scales; for example, one might do daily exercise to achieve a future fitness goal, or resist the temptation of sweets to avoid future weight gain. Damage to the prefrontal cortex often impairs daily decision making, which requires assessment of future outcomes[1,2]. Lesions in the core of the nucleus accumbens in rats result in a tendency to choose small immediate rewards over larger future rewards[3]. Low activity of the central serotonergic system is associated with impulsive behavior in humans[4], and animals with lesions in the ascending serotonergic pathway tend to choose small immediate rewards over larger future rewards[5,6]. A possible mechanism underlying these observations is that different sub-loops of the topographically organized cortico-basal ganglia network are specialized for reward prediction at different time scales and that they are differentially activated by the ascending serotonergic system[7]. To test whether there are distinct neural pathways for reward prediction at different time scales, we developed a 'Markov decision task' in which an action affects not only the immediate reward but also future states and rewards. Using fMRI, we analyzed brain activity in human subjects as they performed this task. Recent functional brain imaging studies have shown the involvement of specific brain areas, such as the orbitofrontal cortex (OFC) and the ventral striatum, in prediction and perception of rewards[8–11]. In these previous studies, however, rewards were given either independent of the subject's actions or as a function of the current action. Our Markov decision task probes decision making in a dynamic context, with small losses followed by a large positive reward. The results of the block-design analysis suggest differential involvement of brain areas in decision making by prediction of rewards at different time scales. By analyzing subjects' performance data according to a theoretical model of reinforcement learning, we found a gradient of activation within the insula and the striatum for prediction of rewards at different time scales.

RESULTS

Behavioral results

In the Markov decision task, a visual signal (one of three shapes) was presented at the start of each trial to indicate one of three states, and the subject selected one of two actions: pressing the right or left button with the right hand (Fig. 1a; see Methods for details). For each state, the subject's action choice affected not only the immediate reward, but also the state subsequently presented (Fig. 1b,c).

The rule of state transition was fixed during the entire experiment (Fig. 1), but the rules of reward delivery changed according to the task condition. In the SHORT condition, action a_1 gives a small positive reward ($+r_1 = 20$ yen average; see Methods) and action a_2 gives a small loss ($-r_1$) in all three states (Fig. 1b). The optimal behavior for maximizing total reward in the SHORT condition is to collect small positive rewards by taking action a_1 at each state. In the LONG condition, action a_2 at state s_3 gives a big bonus ($+r_2 = 100$ yen average; see Methods), and action a_1 at state s_1 results in a big loss ($-r_2$; Fig. 1c). The optimal behavior is to receive small losses at state s_1 and s_2 to obtain a large positive reward at state s_3 by taking action a_2 at each state; this is opposite to the optimal behavior in the SHORT condition. Whereas the optimal strategy in the SHORT condition results in small, immediate rewards at each step, the optimal strategy in the LONG condition results in small immediate losses but a net positive reward by the end of one cycle. Thus, for successful action in the LONG condition, subjects must consider both the

[1]Department of Bioinformatics and Genomics, Nara Institute of Science and Technology, 8916-5 Takayama, Ikoma, Nara 630-0101, Japan. [2]Department of Computational Neurobiology, ATR Computational Neuroscience Laboratories, 2-2-2 Hikaridai, Keihanna Science City, Kyoto 619-0288, Japan. [3]CREST, Japan Science and Technology Agency, 2-2-2 Hikaridai, Keihanna Science City, Kyoto 619-0288, Japan. [4]Department of Psychiatry and Neurosciences, Hiroshima University, 1-2-3 Kasumi, Minamiku, Hiroshima 734-8551, Japan. Correspondence should be addressed to K.D. (doya@atr.jp).

Published online 4 July 2004; doi:10.1038/nn1279

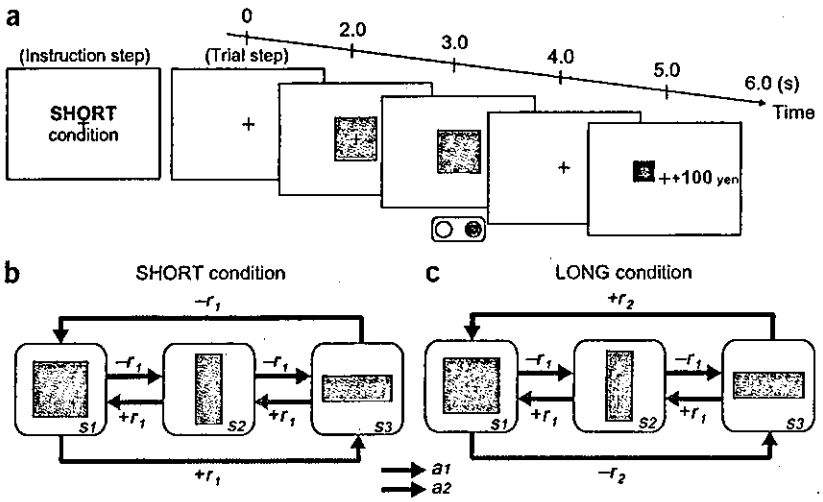

Figure 1 Experimental design. (a) Sequences of stimulus and response events in the task. At the beginning of each condition block, the condition is informed by displaying text (6 s), such as 'SHORT condition' (instruction step). In each trial step, a fixation point is presented on the screen, and after 2 s, one of three shapes (square, vertical rectangle or horizontal rectangle) is presented for 1 s. As the fixation point vanishes after 1 s, the subject presses either the right or left button within 1 s. After a short delay (1 s), a reward for that action is presented by a number (indicating yen gained or lost) and the past cumulative reward is shown by a bar graph. Thus, one trial step takes 6 s. (b,c) The rules of the reward and state transition for action a_1 (magenta arrows) and action a_2 (blue arrows) in the SHORT (b) and LONG (c) conditions. The small reward r_1 was 10, 20 or 30 yen, with equal probability, and the large reward r_2 was 90, 100, or 110 yen. The rule of state transition was the same for all conditions: $s_3 \rightarrow s_2 \rightarrow s_1 \rightarrow s_3 \ldots$ for action a_1, and $s_1 \rightarrow s_2 \rightarrow s_3 \rightarrow s_1 \rightarrow \ldots$ for action a_2. Although the optimal behaviors are opposite (SHORT: a_1; LONG: a_2), the expected cumulative reward during one cycle of the optimal behavior is 60 yen in both the SHORT ($+20 \times 3$) and LONG ($-20, -20, +100$) conditions.

immediate reward and the future reward expected from the subsequent state, and for success in the SHORT condition, subjects need to consider only the immediate outcome of their actions. Subjects performed 15 trials in a SHORT condition block and 15 trials in a LONG condition block. There were also two control conditions, NO (reward was always zero) and RANDOM (reward was $+r_1$ or $-r_1$, regardless of state or action), so a total of four condition blocks were performed (see Fig. 2a for task schedule).

All subjects successfully learned the optimal behaviors: taking action a_1 in the SHORT condition (Fig. 2b) and action a_2 in the LONG condition (Fig. 2c). Cumulative rewards within each SHORT block (Fig. 2d) and LONG block (Fig. 2e) also indicate successful learning. It can be seen from the single-subject data in the LONG condition (Fig. 2e, orange) that the subject learned to lose small amounts ($-r_1$) twice to get a big bonus ($+r_2$). The average cumulative reward in the last block was 254 yen in the SHORT condition and 257 yen in the LONG condition, which was 84.7% and 85.7%, respectively, of the theoretical optimum of 300 yen.

Block-design analysis

To find the brain areas that are involved in immediate reward prediction, we compared brain activity during the SHORT condition and the NO condition, in which reward was always zero. In the SHORT versus NO contrast, a significant increase in activity was observed in the lateral OFC (Fig. 3a), the insula and the occipitotemporal area (OTA) (Fig. 3b), as well as in the striatum, the globus pallidus (GP) (Fig. 3c) and the medial cerebellum (Fig. 3d) (threshold of $P < 0.001$, uncorrected for multiple comparisons). These areas may be involved in reward prediction based on immediate outcome.

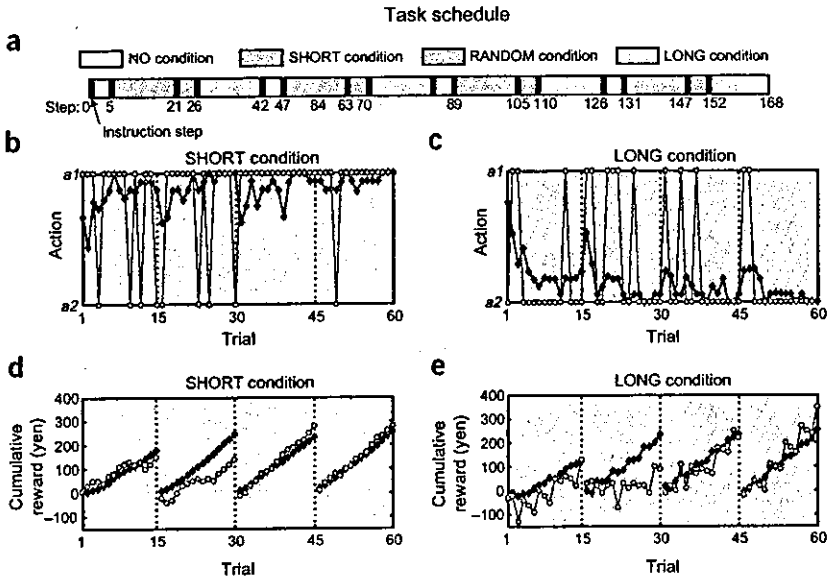

Figure 2 Task schedule and behavioral results. (a) A set of four condition blocks—NO (4 trials), SHORT (15 trials), RANDOM (4 trials), LONG (15 trials)—was repeated four times. At the beginning of each condition block, the task condition was presented to the subject (instruction step); thus, the entire experiment consisted of 168 steps (152 trial steps and 16 instruction steps). (b,c) The selected action of a representative single subject (orange) and the group average ratio of selecting a_1 (blue) in the (b) SHORT and (c) LONG conditions. (d,e) The accumulated reward in each block of a representative single subject (orange) and the group average (blue) in the (d) SHORT and (e) LONG conditions. To clearly show the learning effects, data from four trial blocks in the SHORT and LONG conditions are concatenated, with the dotted lines indicating the end of each condition block.

To identify areas involved in future reward prediction, we compared the brain activity during LONG and SHORT conditions. In the LONG versus SHORT contrast, a robust increase in activity was observed in the ventrolateral prefrontal cortex (VLPFC), the insula, the dorsolateral prefrontal cortex (DLPFC), the dorsal premotor cortex (PMd), the inferior parietal cortex (IPC) (Fig. 4a), the striatum, GP (Fig. 4b), the dorsal raphe nucleus (Fig. 4c), the lateral cerebellum (Fig. 4d), the posterior cingulate cortex and the subthalamic nucleus ($P < 0.001$, uncorrected). Activity in the striatum was highly significant (threshold at $P < 0.05$, corrected for a small volume when using an anatomically defined region of interest (ROI) in the striatum; see Methods). These areas are specifically involved in decision making based on the prediction of reward in multiple steps in the future. In the LONG versus NO contrast, the activated areas were approximately the union of the areas activated in the SHORT versus NO and LONG versus SHORT contrasts. These results were consistent with our expectation that both immediate and future reward prediction were required in the LONG condition. The results of block-design analysis, including the LONG versus NO contrast, are summarized in Supplementary Table 1 online. Activitions in both SHORT and LONG conditions were stronger in the first two blocks, when subjects were involved in active trial and error, than in the last two blocks when the subjects' behavior became repetitive.

We compared the activitions in the SHORT versus NO contrast and the LONG versus SHORT contrast, and observed that three regions showed significant activity in both contrasts: the lateral prefrontal cortex (lateral OFC and VLPFC), the insula and the anterior striatum (Fig. 5). In the lateral PFC (Fig. 5a), although the activities in lateral OFC for the SHORT versus NO contrast (red) and in the VLPFC for the LONG versus SHORT contrast (blue) were close in location, they were clearly separated on the cortical surface. Activities in the insula were also separated (Fig. 5b). In the anterior striatum (Fig. 5c), we found limited overlaps between the two contrasts (green). In all three areas, activations in the SHORT versus NO contrast were found in the ventral parts, whereas activations in the LONG versus SHORT contrast were found in the dorsal parts.

These results of block-design analysis suggest differential involvement of brain areas in predicting immediate and future rewards.

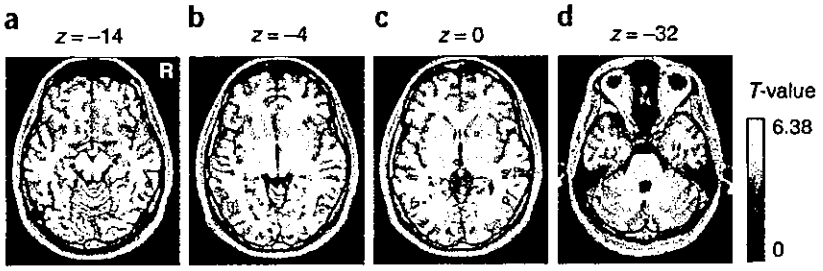

Figure 3 Brain areas activated in the SHORT versus NO contrast ($P < 0.001$, uncorrected; extent threshold of four voxels). (a) Lateral OFC. (b) Insula. (c) Striatum. (d) Medial cerebellum.

Performance-based multiple regression analysis

To further clarify the brain structures specific to reward prediction at different time scales, we estimated how much reward the subjects should have predicted on the basis of their performance data and used their time courses as the explanatory variables of regression analysis. We took the theoretical framework of temporal difference (TD) learning[12], which has been successfully used for explaining reward-predictive activations of the midbrain dopaminergic system as well as those of the cortex and the striatum[8,11,13–16]. In TD learning theory, the predicted amount of future reward starting from a state $s(t)$ is formulated as the 'value function'

$$V(t) = E[r(t+1) + \gamma r(t+2) + \gamma^2 r(t+3) + \ldots]. \quad (1)$$

Any deviation from the prediction is given by the TD error

$$\delta(t) = r(t) + \gamma V(t) - V(t-1), \quad (2)$$

which is a crucial learning signal for reward prediction and action selection. The 'discount factor' γ ($0 \leq \gamma < 1$) controls the time scale of prediction: when $\gamma = 0$, only the immediate reward $r(t+1)$ is considered, but as γ approaches 1, rewards in the further future are taken into account.

We estimated the time courses of reward prediction $V(t)$ and prediction error $\delta(t)$ from each subject's performance data and used them as the explanatory variables in multiple regression analysis with fMRI data (see Methods). In our Markov decision task, the minimum value of γ needed to find the optimal action in the LONG condition is 0.36, and any small value of γ is sufficient in the SHORT condition. From the results of our block-design analysis, we assumed that different networks involving the cortex and basal ganglia are specialized for reward prediction at different time scales and that they work in parallel, depending on the requirement of the task. Thus, we varied the discount factor γ as 0, 0.3, 0.6, 0.8, 0.9 and 0.99: small γ for immediate reward prediction and large γ for long future reward prediction. An example of these time courses is shown in Supplementary Figure 1 online.

We observed a significant correlation with reward prediction $V(t)$ in the medial prefrontal cortex (mPFC; including the anterior cingulate cortex (ACC) and the medial OFC) (Fig. 6a) and bilateral insula (Fig. 6b), left hippocampus and left temporal pole ($P < 0.001$, uncorrected; see Supplementary Table 2 online). Figure 6 shows the correlated

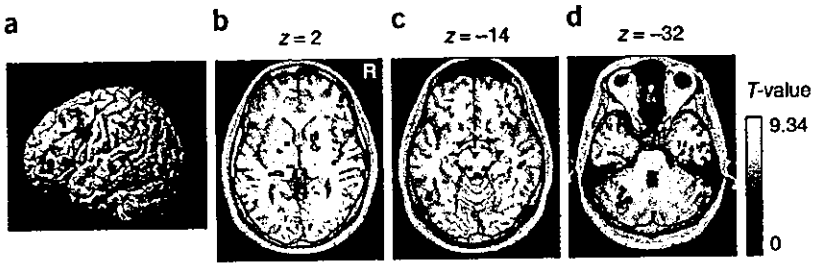

Figure 4 Brain areas activated in the LONG versus SHORT contrast ($P < 0.0001$, uncorrected; extent threshold of four voxels for illustration purposes). (a) DLPFC, IPC, PMd. (b) GP, striatum. (c) Dorsal raphe nucleus. (d) Left lateral cerebellum.

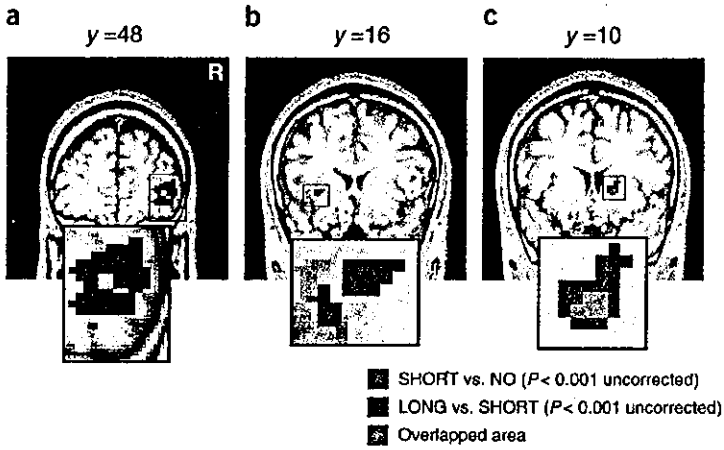

Figure 5 Comparison of brain areas activated in the SHORT versus NO contrast (red) and the LONG versus SHORT contrast (blue). (a–c) These figures show activation maps focused on (a) the lateral OFC (red (x, y, z) = (38, 46, −14); blue (46, 47, 3)) (b) the insula (red (−36, 13, −4); blue (−30, 18, 1)), and (c) the striatum (red (18, 10, 0); blue (18, 12, 3)) where we observed significant activation in both contrasts. The areas where activity overlapped area are shown in green.

voxels within these areas using a gradient of colors for different γ values (red for $\gamma = 0$, blue for $\gamma = 0.99$). Activity in the mPFC, temporal pole and hippocampus correlated with reward prediction with a longer time scale ($\gamma \geq 0.6$). Furthermore, in the insula, we found a graded map of activity for reward prediction at different time scales (Fig. 6b). Whereas activity in the ventroanterior region correlated with reward prediction at a shorter time scale, activity in the dorsoposterior region correlated with reward prediction at a longer time scale.

We also found, in the basal ganglia, significant correlation with reward prediction error $\delta(t)$ using a wide range of time scales (Fig. 6c; $P < 0.001$, uncorrected; see Supplementary Table 3 online and Methods). Again, we found a graded map, which had a short time scale in the ventroanterior part and a long time scale in the dorsoposterior part. The coincidence of the ventroanterior-dorsoposterior maps and the ventroanterior-dorsoposterior shifts in activities (Fig. 6b,c) indicate that, while the ventroanterior regions with smaller γ were predominantly active in the SHORT condition, the dorsoposterior regions with larger γ became more active in the LONG condition.

DISCUSSION

The results of the block-design and performance-based regression analyses suggest differential involvement of brain areas in action learning by prediction of rewards at different time scales. Both block-design and performance-based regression analyses showed activity in the insula and the anterior striatum. Activations of the ventral region in the SHORT versus NO contrast and the dorsal region in the LONG versus SHORT contrast in each area (Fig. 5) are consistent with the ventroanterior-dorsoposterior maps of the discount factor γ found in performance-based regression analysis (Fig. 6).

The insula takes a pivotal position in reward processing by receiving primary taste and visceral sensory input[17] and sending output to the OFC[18] and the striatum[19]. Previous studies showed that the insula is activated with anticipation of primary reward[10] and that insular lesion causes deficits in incentive learning for primary reward[20]. Our results confirm the role of the insula in prediction of non-primary, monetary reward[21], and further suggest heterogeneous organization within the insula. Previous imaging studies also showed involvement of the insula, especially the ventroanterior region, in processing aversive outcomes[22,23]. Thus a possible interpretation of the activation of the insula in the LONG condition is that it

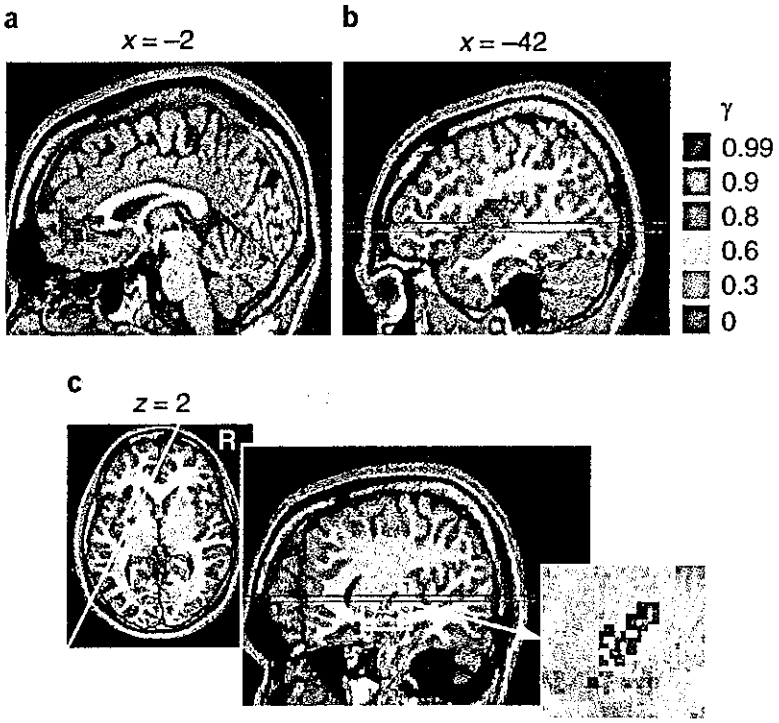

Figure 6 Voxels with a significant correlation (height threshold $P < 0.001$, uncorrected; extent threshold of four voxels) with reward prediction $V(t)$ and prediction error $\delta(t)$ are shown in different colors for different settings of the discount factor γ. Voxels correlated with two or more regressors are shown by a mosaic of colors. (a, b) Significant correlation with reward prediction $V(t)$. (a) mPFC. (b) Insula. (c) Significant correlation with reward prediction error $\delta(t)$ restricted to ROI in the striatum (slice at white line in horizontal slice at $z = 2$ mm). Note the ventroanterior-to-dorsoposterior gradient with the increase in γ both in the insula and the striatum. Red and blue lines correspond to the z-coordinate levels of activation peaks in the insula and striatum shown in Figure 5b,c (red for the SHORT versus NO and blue for the LONG versus SHORT contrasts).

reflected the losses that subjects acquired before getting a large reward. However, we also ran a regression analysis using losses and found significant correlation in the ventroanterior region of the insula. Anatomical and physiological studies of the insula also showed involvement of its ventroanterior part in perception of aversive stimuli[17]. Thus we argue that the activation of dorsoposterior insula is not simply due to losses in the LONG condition.

Previous brain imaging and neural recording studies suggest a role for the striatum in prediction and processing of reward[9,10,14,21,24–29]. Consistent with previous fMRI studies[8,11,16], our results showed striatal activity correlated with the error of reward prediction. Reinforcement learning models of the basal ganglia[13–15] posit that the striatum learns reward prediction and action selection based on the reward prediction error $\delta(t)$ represented by the dopaminergic input. Correlation of striatal activity with reward prediction error $\delta(t)$ could be due to dopamine-dependent plasticity of cortico-striatal synapses[30].

In lateral OFC, DLPFC, PMd, IPC and dorsal raphe, we found significant activations in the block-design analyses, but we did not find strong correlation in regression analyses. This may be because these areas perform functions that are helpful for reward prediction and action selection, but their activities do not directly represent the amount of predicted reward or prediction error at a specific time scale.

In reinforcement learning theory, an optimal action selection is realized by taking the action a that maximizes the 'action value' $Q(s, a)$ at a given state s. The action value is defined as $Q(s, a) = E[\, r(s, a) + \gamma V(s'(s, a))]$ and represents the expected sum of the immediate reward $r(s, a)$ and the weighted future rewards $V(s'(s, a))$, where $s'(s, a)$ means the next state reached by taking an action a at a state s (refs. 12,15). According to this framework, we can see that prediction of immediate reward $r(s, a)$ is helpful for action selection based on rewards at either short or long time scales, that is, with any value of the discount factor γ. On the other hand, prediction of state transition $s'(s, a)$ is helpful only in long-term reward prediction with positive values of γ.

In the lateral OFC, we observed significant activity in both the SHORT versus NO and the LONG versus NO contrasts (Supplementary Table 1 online), but no significant correlation with reward prediction $V(t)$ or reward prediction error $\delta(t)$ in regression analysis. This suggests that the lateral OFC takes the role of predicting immediate reward $r(s, a)$, which is used for action selection in both SHORT and LONG conditions, but not in the NO condition. This interpretation is consistent with previous studies demonstrating the OFC's role in prediction of rewards, immediately following sensorimotor events[31,32], and action selection based on reward prediction[23,33,34].

In the DLPFC, PMd and IPC, there were significant activations in both the LONG versus NO and the LONG versus SHORT contrasts (Supplementary Table 1 online) but no significant correlation with either $V(t)$ or $\delta(t)$. A possible interpretation is that this area is involved in prediction of future state $s'(s, a)$ in the LONG condition but not in the SHORT or NO conditions. This interpretation is consistent with previous studies showing the role of these cortical areas in imagery[35], working memory and planning[36,37].

The dorsal raphe nucleus was activated in the LONG versus SHORT contrast, but was not correlated with $V(t)$ or $\delta(t)$. In consideration of its serotonergic projection to the cortex and the striatum and serotonin's implication with behavioral impulsivity[4–6], a possible role for the dorsal raphe nucleus is to control the effective time scale of reward prediction[7]. Its higher activity in the LONG condition, where a large setting of γ is necessary, is consistent with this hypothesis.

Let us consider the present experimental results in light of the anatomy of cortico-basal ganglia loops (illustrated in Supplementary Fig. 2). The cortex and the basal ganglia both have parallel loop organization, with four major loops (limbic, cognitive, motor and oculomotor) and finer, topographic sub-loops within each major loop[38]. Our results suggest that the areas within the limbic loop[39], namely the lateral OFC and ventral striatum, are involved in immediate reward prediction. On the other hand, areas within the cognitive and motor loops[38], including the DLPFC, IPC, PMd and dorsal striatum, are involved in future reward prediction. The connections from the insula to the striatum are topographically organized, with the ventral-anterior, agranular cortex projecting to the ventral striatum and the dorsal-posterior, granular cortex projecting to the dorsal striatum[19] (see Supplementary Fig. 2). The graded maps shown in Figure 6b,c are consistent with this topographic cortico-striatal organization and suggest that areas that project to the more dorsoposterior part of the striatum are involved in reward prediction at a longer time scale. These results are consistent with the observations that localized damages within the limbic and cognitive loops manifest as deficits in evaluation of future rewards[1,3,34,40,41] and learning of multi-step behaviors[42]. The parallel learning mechanisms in the cortico-basal ganglia loops used for reward prediction at a variety of time scales may have the merit of enabling flexible selection of a relevant time scale appropriate for the task and the environment at the time of decision making.

A possible mechanism for selection or weighting of different cortico-basal ganglia loops with an appropriate time scale is serotonergic projection from the dorsal raphe nucleus[7] (see Supplementary Fig. 2), which was activated in the LONG versus SHORT contrast. Although serotonergic projection is supposed to be diffuse and global, differential expression of serotonergic receptors in the cortical areas and in the ventral and dorsal striatum[43,44] would result in differential modulation. The mPFC, which had significant correlation with reward prediction $V(t)$ at long time scales ($\gamma \geq 0.6$), may regulate the activity of the raphe nucleus through reciprocal connection[45,46]. This interpretation is consistent with previous studies using tasks that require long-range prospects for problem solving, such as the gambling problem[1] or delayed reward task[2], which showed involvement of the medial OFC. Future studies using the Markov decision task under pharmacological manipulation of the serotonergic system should clarify the role of serotonin in regulating the time scale of reward prediction.

Recent brain imaging and neural recording studies report involvement of a variety of cortical areas and the striatum in reward processing[8–11,16,21,23–29,32,33,47–49]. Although some neural recording studies have used experimental tasks that require multiple trial steps for getting rewards[47,48], none of the previous functional brain imaging studies addressed the issue of reward prediction at different time scales, and considered only rewards immediately following stimuli or actions. We were able extract specific functions of OFC, DLPFC, mPFC, insula and cortico-basal ganglia loops using our new Markov decision task and a reinforcement learning model–based regression analysis. Our regression analysis not only extracted brain activities specific to reward prediction, but also revealed a topographic organization in reward prediction (Fig. 6). The combination of our Markov decision task with event-related fMRI and magnetoencephalography (MEG) should further clarify the functions used for reward prediction and perception at different time scales, and at finer spatial and temporal resolutions.

METHODS

Subjects. Twenty healthy, right-handed volunteers (18 males and 2 females, ages 22–34 years) gave informed consent to participate in the experiment, which was conducted with the approval of the ethics and safety committees of Advanced Telecommunication Research Institute International (ATR) and Hiroshima University.

Behavioral task. In the Markov decision task (Fig. 1), one of three states was visually presented to the subject using three different shapes, and the subject selected one of two actions by pressing one of two buttons using their right hand (Fig. 1a). The rule of state transition was the same for all conditions: $s_3 \rightarrow s_2 \rightarrow s_1 \rightarrow s_3 \sim$. for action a_1, and $s_1 \rightarrow s_2 \rightarrow s_3 \rightarrow s_1 \rightarrow \ldots$ for action a_2. The rules for reward, however, changed in each condition. In the SHORT condition (Fig. 1b), action a_1 results in a small positive reward ($+r_1$ = 10, 20 or 30 yen, with equal probabilities), whereas action a_2 results in a small loss ($-r_1$) at any of the three states. Thus, the optimal behavior is to collect small positive rewards at each state by performing action a_1. In the LONG condition (Fig. 1c), however, the reward setting is such that action a_2 gives a large positive reward ($+r_2$ = 90, 100 or 110 yen) at state s_3, and action a_1 gives a large loss ($-r_2$) at state s_1. Thus, the optimal behavior is to receive small losses at states s_1 and s_2 to obtain a large positive reward at state s_3 by taking action a_2 at each state. There were two control conditions: the NO condition, where the reward was always zero, and the RANDOM condition, where the reward was positive ($+r_1$) or negative ($-r_1$) with equal probability, regardless of state or action.

Subjects completed 4 trials in a NO condition block, 15 trials in a SHORT condition block, 4 trials in a RANDOM condition block and 15 trials in a LONG condition block. A set of four condition blocks (NO, SHORT, RANDOM, LONG) was repeated four times (Fig. 2a). Subjects were informed of the current condition at the beginning of each condition block by text on the screen (first slide in Fig. 1a); thus, the entire experiment consisted of 168 steps (152 trial steps and 16 instruction steps), taking about 17 min. The mappings of the three states to the three figures, and the two buttons to the two actions, were randomly set at the beginning of each experiment, so that subjects were required to learn the amount of reward associated with each figure-button pair in both SHORT and LONG conditions. Furthermore, in the LONG condition, subjects had to learn the subsequent figure for each figure-action pair and take into account the amount of reward expected from the subsequent figure in selecting a button.

fMRI imaging. A 1.5-tesla scanner (Shimadzu-Marconi, Magnex Eclipse) was used to acquire both structural T1-weighted images (repetition time, TR = 12 ms, TE = 4.5 ms, flip angle = 20°, matrix = 256 × 256, FoV = 256 mm, thickness = 1 mm, slice gaP = 0 mm) and T2*-weighted echo planar images (TR = 6 s, TE = 55 ms, flip angle = 90°, 50 transverse slices, matrix = 64 × 64, FoV = 192 mm, thickness = 3 mm, slice gap = 0 mm) showing blood oxygen level–dependent (BOLD) contrasts.

Because the aim of the present study was to identify brain activity underlying reward prediction over multiple trial steps, we acquired functional images every 6 s (TR = 6 s), in synchrony with single trials. Although shorter TRs and event-related designs are often used in experiments that aim to distinguish brain responses to events within a trial[9,11,21,26], analysis of those finer events in time were not the focus of the current study. With this longer TR, the BOLD signal in a single scan contained a mixture of responses for a reward-predictive stimulus and reward feedback. However, because of the progress of learning and the stochastic nature of the amount of reward, the time courses of reward prediction $V(t)$ and prediction error $\delta(t)$ over the 168 trial steps were markedly different. Thus, we could separate activity corresponding to reward prediction from that corresponding to outcomes by using both reward prediction $V(t)$ and reward outcome $r(t)$ in multiple regression analysis, as described below.

Data analysis. The data were pre-processed and analyzed with SPM99 (www.fil.ion.ucl.ac.uk/spm/spm99.html). The first two volumes of images were discarded to avoid T1 equilibrium effects. The images were realigned to the first image as a reference, spatially normalized with respect to the Montreal Neurological Institute EPI template, and spatially smoothed with a Gaussian kernel (8 mm, full-width at half-maximum).

We conducted two types of analysis. One was block-design analysis using four boxcar regressors covering the whole experiment, convolved with a hemodynamic response function as the reference waveform for each condition (NO, SHORT, RANDOM, LONG). We did not find substantial differences between SHORT versus NO and SHORT versus RANDOM contrasts, or between LONG versus NO and LONG versus RANDOM contrasts. Therefore we report here only the results with the NO condition as the control condition. The other method was multivariate regression analysis using explanatory variables, representing the time course of the reward prediction $V(t)$ or reward prediction error $\delta(t)$ at six different timescales γ, estimated from subjects' performance data (described below).

In both analyses, images of parameter estimates for the contrast of interest were created for each subject. These were then entered into a second-level group analysis using a one-sample t test at a threshold of $P < 0.001$, uncorrected for multiple comparisons (random effects analysis) and extent threshold of four voxels. Small-volume correction (SVC) was done at a threshold of $P < 0.05$ using an ROI within the striatum (including the caudate and putamen), which was defined anatomically based on a normalized T1 image.

Procedures of performance-based regression analysis. The time courses of reward prediction $V(t)$ and reward prediction error $\delta(t)$ were estimated from each subject's performance data—state $s(t)$, action $a(t)$ and reward $r(t)$—as described below.

Reward prediction. To estimate how much of a forthcoming reward a subject would have expected at each step during the Markov decision task, we took the definition of the value function (equation 1) and reformulated it based on the recursive structure of the task. Namely, if the subject starts from a state $s(t)$ and comes back to the same state after k steps, the expected cumulative reward $V(t)$ should satisfy the consistency condition $V(t) = r(t+1) + \gamma\, r(t+2) + \ldots + \gamma^{k-1} r(t+k) + \gamma^k V(t)$.

Thus, for each time t of the data file, we calculated the weighted sum of the rewards acquired until the subject returned to the same state and estimated the value function for that episode as

$$\hat{V}(t) = \frac{\left[r(t+1) + \gamma r(t+2) + \Lambda + \gamma^{k-1} r(t+k)\right]}{1-\gamma^k} \qquad (1)$$

The estimate of the value function $V(t)$ at time t was given by the average of all previous episodes from the same state as at time t

$$V(t) = \frac{1}{L}\sum_{i=1}^{L} \hat{V}(t_i) \qquad (2)$$

where $\{t_1, \ldots, t_L\}$ are the indices of time visiting the same state as $s(t)$, that is, $s(t_1) = \ldots = s(t_L) = s(t)$.

Reward prediction error. The TD error (equation 2) was calculated from the difference between the actual reward $r(t)$ and the temporal difference of the estimated value function $V(t)$.

We separately calculated the time courses of $V(t)$ and $\delta(t)$ during SHORT and LONG conditions; we concatenated data of four blocks in the SHORT condition, and calculated $V(t)$ and $\delta(t)$ as described above. We used the same process for the LONG condition data. During the NO and RANDOM conditions, the values of $V(t)$ and $\delta(t)$ were fixed at zero. Finally, we reconstructed the data corresponding to the real time course of the experiment. Examples of the time course of these variables are shown in Supplementary Figure 1 online. We used either $V(t)$ or $\delta(t)$ as the explanatory variable in a regression analysis by SPM. To remove any effects of factors other than reward prediction, we concurrently used other variables in the regression, namely the four box-car functions representing each condition (NO, SHORT, RANDOM, LONG). Because the immediate reward prediction $V(t)$ with $\gamma = 0$ can coincide with reward outcome $r(t)$ if learning is perfect, we included the reward outcome $r(t)$ in regression analyses with $V(t)$. Thus, the significant correlation with $V(t)$ (Fig. 6a,b) should represent a predictive component rather than a reward outcome.

The amplitude of explanatory variables $\delta(t)$ with all γ were large in early trials and decreased as subjects learned the task (Supplementary Fig. 1 online). This decreasing trend causes a risk that areas that are activated early in trials, such as those responsible for general attentiveness or novelty, have correlations with $\delta(t)$. Because our aim in regression analysis was to clarify the brain structures involved in reward prediction at specific time scales, we removed the areas that had similar correlation to $\delta(t)$ at all settings of γ from considerations in Figure 6 and Supplementary Table 3 online. To compare the results of regression analysis

with six different values of γ, we used display software that can overlay multiple activation maps in different colors on a single brain structure image. When a voxel is significantly activated in multiple values of γ, it is shown by a mosaic of multiple colors, with apparent subdivision of the voxel (Fig. 6).

Note: Supplementary information is available on the Nature Neuroscience website.

ACKNOWLEDGMENTS

We thank K. Samejima, N. Schweighofer, M. Haruno, H. Imamizu, S. Higuchi, T. Yoshioka, T. Chaminade and M. Kawato for helpful discussions and technical advice. This research was funded by 'Creating the Brain,' Core Research for Evolutional Science and Technology (CREST), Japan Science and Technology Agency.

COMPETING INTERESTS STATEMENT

The authors declare that they have no competing financial interests.

Received 5 March; accepted 2 June 2004
Published online at http://www.nature.com/natureneuroscience/

1. Bechara, A., Damasio, H. & Damasio, A.R. Emotion, decision making and the orbitofrontal cortex. *Cereb. Cortex* **10**, 295–307 (2000).
2. Mobini, S. *et al.* Effects of lesions of the orbitofrontal cortex on sensitivity to delayed and probabilistic reinforcement. *Psychopharmacology (Berl.)* **160**, 290–298 (2002).
3. Cardinal, R.N., Pennicott, D.R., Sugathapala, C.L., Robbins, T.W. & Everitt, B.J. Impulsive choice induced in rats by lesions of the nucleus accumbens core. *Science* **292**, 2499–2501 (2001).
4. Rogers, R.D. *et al.* Dissociable deficits in the decision-making cognition of chronic amphetamine abusers, opiate abusers, patients with focal damage to prefrontal cortex, and tryptophan-depleted normal volunteers: evidence for monoaminergic mechanisms. *Neuropsychopharmacology* **20**, 322–339 (1999).
5. Evenden, J.L. & Ryan, C.N. The pharmacology of impulsive behaviour in rats: the effects of drugs on response choice with varying delays of reinforcement. *Psychopharmacology (Berl.)* **128**, 161–170 (1996).
6. Mobini, S., Chiang, T.J., Ho, M.Y., Bradshaw, C.M. & Szabadi, E. Effects of central 5-hydroxytryptamine depletion on sensitivity to delayed and probabilistic reinforcement. *Psychopharmacology (Berl.)* **152**, 390–397 (2000).
7. Doya, K. Metalearning and neuromodulation. *Neural Net.* **15**, 495–506 (2002).
8. Berns, G.S., McClure, S.M., Pagnoni, G. & Montague, P.R. Predictability modulates human brain response to reward. *J. Neurosci.* **21**, 2793–2798 (2001).
9. Breiter, H.C., Aharon, I., Kahneman, D., Dale, A. & Shizgal, P. Functional imaging of neural responses to expectancy and experience of monetary gains and losses. *Neuron* **30**, 619–639 (2001).
10. O'Doherty, J.P., Deichmann, R., Critchley, H.D. & Dolan, R.J. Neural responses during anticipation of a primary taste reward. *Neuron* **33**, 815–826 (2002).
11. O'Doherty, J.P., Dayan, P., Friston, K., Critchley, H. & Dolan, R.J. Temporal difference models and reward-related learning in the human brain. *Neuron* **38**, 329–337 (2003).
12. Sutton, R.S. & Barto, A.G. *Reinforcement Learning* (MIT Press, Cambridge, Massachusetts, 1998).
13. Houk, J.C., Adams, J.L. & Barto, A.G. in *Models of Information Processing in the Basal Ganglia* (eds. Houk, J.C., Davis, J.L. & Beiser, D.G.) 249–270 (MIT Press, Cambridge, Massachusetts, 1995).
14. Schultz, W., Dayan, P. & Montague, P.R. A neural substrate of prediction and reward. *Science* **275**, 1593–1599 (1997).
15. Doya, K. Complementary roles of basal ganglia and cerebellum in learning and motor control. *Curr. Opin. Neurobiol.* **10**, 732–739 (2000).
16. McClure, S.M., Berns, G.S. & Montague, P.R. Temporal prediction errors in a passive learning task activate human striatum. *Neuron* **38**, 339–346 (2003).
17. Mesulam, M.M. & Mufson, E.J. Insula of the old world monkey. III: Efferent cortical output and comments on function. *J. Comp. Neurol.* **212**, 38–52 (1982).
18. Cavada, C., Company, T., Tejedor, J., Cruz-Rizzolo, R.J. & Reinoso-Suarez, F. The anatomical connections of the macaque monkey orbitofrontal cortex. *Cereb. Cortex* **10**, 220–242 (2000).
19. Chikama, M., McFarland, N.R., Amaral, D.G. & Haber, S.N. Insular cortical projections to functional regions of the striatum correlate with cortical cytoarchitectonic organization in the primate. *J. Neurosci.* **17**, 9686–9705 (1997).
20. Balleine, B.W. & Dickinson, A. The effect of lesions of the insular cortex on instrumental conditioning: evidence for a role in incentive memory. *J. Neurosci.* **20**, 8954–8964 (2000).
21. Knutson, B., Fong, G.W., Bennett, S.M., Adams, C.M. & Hommer, D. A region of mesial prefrontal cortex tracks monetarily rewarding outcomes: characterization with rapid event-related fMRI. *Neuroimage* **18**, 263–272 (2003).
22. Ullsperger, M. & von Cramon, D.Y. Error monitoring using external feedback: specific roles of the habenular complex, the reward system, and the cingulate motor area revealed by functional magnetic resonance imaging. *J. Neurosci.* **23**, 4308–4314 (2003).
23. O'Doherty, J., Critchley, H., Deichmann, R. & Dolan, R.J. Dissociating valence of outcome from behavioral control in human orbital and ventral prefrontal cortices. *J. Neurosci.* **23**, 7931–7939 (2003).
24. Koepp, M.J. *et al.* Evidence for striatal dopamine release during a video game. *Nature* **393**, 266–268 (1998).
25. Elliott, R., Friston, K.J. & Dolan, R.J. Dissociable neural responses in human reward systems. *J. Neurosci.* **20**, 6159–6165 (2000).
26. Knutson, B., Adams, C.M., Fong, G.W. & Hommer, D. Anticipation of increasing monetary reward selectively recruits nucleus accumbens. *J. Neurosci.* **21**, RC159 (2001).
27. Pagnoni, G., Zink, C.F., Montague, P.R. & Berns, G.S. Activity in human ventral striatum locked to errors of reward prediction. *Nat. Neurosci.* **5**, 97–98 (2002).
28. Elliott, R., Newman, J.L., Longe, O.A. & Deakin, J.F. Differential response patterns in the striatum and orbitofrontal cortex to financial reward in humans: a parametric functional magnetic resonance imaging study. *J. Neurosci.* **23**, 303–307 (2003).
29. Haruno, M. *et al.* A neural correlate of reward-based behavioral learning in caudate nucleus: a functional magnetic resonance imaging study of a stochastic decision task. *J. Neurosci.* **24**, 1660–1665 (2004).
30. Reynolds, J.N. & Wickens, J.R. Dopamine-dependent plasticity of corticostriatal synapses. *Neural Net.* **15**, 507–521 (2002).
31. Tremblay, L. & Schultz, W. Reward-related neuronal activity during go-nogo task performance in primate orbitofrontal cortex. *J. Neurophysiol.* **83**, 1864–1876 (2000).
32. Critchley, H.D., Mathias, C.J. & Dolan, R.J. Neural activity in the human brain relating to uncertainty and arousal during anticipation. *Neuron* **29**, 537–545 (2001).
33. Rogers, R.D. *et al.* Choosing between small, likely rewards and large, unlikely rewards activates inferior and orbital prefrontal cortex. *J. Neurosci.* **19**, 9029–9038 (1999).
34. Rolls, E.T. The orbitofrontal cortex and reward. *Cereb. Cortex* **10**, 284–294 (2000).
35. Hanakawa, T. *et al.* The role of rostral Brodmann area 6 in mental-operation tasks: an integrative neuroimaging approach. *Cereb. Cortex* **12**, 1157–1170 (2002).
36. Owen, A.M., Doyon, J., Petrides, M. & Evans, A.C. Planning and spatial working memory: a positron emission tomography study in humans. *Eur. J. Neurosci.* **8**, 353–364 (1996).
37. Baker, S.C. *et al.* Neural systems engaged by planning: a PET study of the Tower of London task. *Neuropsychologia* **34**, 515–526 (1996).
38. Middleton, F.A. & Strick, P.L. Basal ganglia and cerebellar loops: motor and cognitive circuits. *Brain Res. Brain Res. Rev.* **31**, 236–250 (2000).
39. Haber, S.N., Kunishio, K., Mizobuchi, M. & Lynd-Balta, E. The orbital and medial prefrontal circuit through the primate basal ganglia. *J. Neurosci.* **15**, 4851–4867 (1995).
40. Eagle, D.M., Humby, T., Dunnett, S.B. & Robbins, T.W. Effects of regional striatal lesions on motor, motivational, and executive aspects of progressive-ratio performance in rats. *Behav. Neurosci.* **113**, 718–731 (1999).
41. Pears, A., Parkinson, J.A., Hopewell, L., Everitt, B.J. & Roberts, A.C. Lesions of the orbitofrontal but not medial prefrontal cortex disrupt conditioned reinforcement in primates. *J. Neurosci.* **23**, 11189–11201 (2003).
42. Hikosaka, O. *et al.* Parallel neural networks for learning sequential procedures. *Trends Neurosci.* **22**, 464–471 (1999).
43. Mijnster, M.J. *et al.* Regional and cellular distribution of serotonin 5-hydroxytryptamine2a receptor mRNA in the nucleus accumbens, olfactory tubercle, and caudate putamen of the rat. *J. Comp. Neurol.* **389**, 1–11 (1997).
44. Compan, V., Segu, L., Buhot, M.C. & Daszuta, A. Selective increases in serotonin 5-HT1B/1D and 5-HT2A/2C binding sites in adult rat basal ganglia following lesions of serotonergic neurons. *Brain Res.* **793**, 103–111 (1998).
45. Celada, P., Puig, M.V., Casanovas, J.M., Guillazo, G. & Artigas, F. Control of dorsal raphe serotonergic neurons by the medial prefrontal cortex: involvement of serotonin-1A, GABA(A), and glutamate receptors. *J. Neurosci.* **21**, 9917–9929 (2001).
46. Martin-Ruiz, R. *et al.* Control of serotonergic function in medial prefrontal cortex by serotonin-2A receptors through a glutamate-dependent mechanism. *J. Neurosci.* **21**, 9856–9866 (2001).
47. Hikosaka, K. & Watanabe, M. Delay activity of orbital and lateral prefrontal neurons of the monkey varying with different rewards. *Cereb. Cortex* **10**, 263–271 (2000).
48. Shidara, M. & Richmond, B.J. Anterior cingulate: single neuronal signals related to degree of reward expectancy. *Science* **296**, 1709–1711 (2002).
49. Matsumoto, K., Suzuki, W. & Tanaka, K. Neuronal correlates of goal-based motor selection in the prefrontal cortex. *Science* **301**, 229–232 (2003).

Effects of Changing From Typical to Atypical Antipsychotic Drugs on Subjective Sleep Quality in Patients With Schizophrenia in a Japanese Population

Hidehisa Yamashita, M.D., Ph.D.; Kazuhiko Mori, M.D., Ph.D.; Masatsugu Nagao, M.D., Ph.D.; Yasumasa Okamoto, M.D., Ph.D.; Shigeru Morinobu, M.D., Ph.D.; and Shigeto Yamawaki, M.D., Ph.D.

Objective: To investigate the effects of the atypical antipsychotic drugs risperidone, olanzapine, quetiapine, and perospirone on the subjective quality of sleep in patients with schizophrenia.

Method: Subjects were 92 inpatients (mean age = 59.9 years) who had been receiving treatment with conventional antipsychotic drugs and who met the DSM-IV criteria for schizophrenia. Subjects were randomly assigned to receive 1 of 4 atypical antipsychotic drugs (olanzapine, perospirone, quetiapine, and risperidone). Subjective sleep quality and psychopathology were assessed twice: at baseline and 8 weeks after switching. Data were collected from June 2001 to December 2001. Subjective sleep quality was assessed by the Pittsburgh Sleep Quality Index (PSQI), and psychopathology was measured by the Positive and Negative Syndrome Scale (PANSS).

Results: Subjective sleep quality as assessed by the PSQI was significantly improved with administration of olanzapine, risperidone, or quetiapine, but not with perospirone, in comparison with conventional antipsychotic drugs. Multiple regression analysis revealed that the improvement of sleep quality with administration of atypical antipsychotic drugs was predicted by poor sleep quality at baseline. In addition, improvement of sleep quality was significantly correlated with improvement of negative symptoms as assessed by the PANSS.

Conclusion: These results demonstrated that atypical antipsychotic drugs improved subjective quality of sleep in patients with schizophrenia compared with conventional antipsychotic drugs, suggesting that the marked potency of serotonin-2 receptor blockade in atypical antipsychotic drugs may be involved in the mechanism of this improvement. These improvements were correlated with improvement of negative symptoms.

(J Clin Psychiatry 2004;65:1525–1530)

Received Oct. 25, 2003; accepted March 30, 2004. *From the Department of Psychiatry and Neurosciences, Graduate School of Biomedical Sciences Hiroshima University, Hiroshima (Drs. Yamashita, Mori, Okamoto, Morinobu, and Yamawaki); Core Research for Evolutional Science and Technology (CREST) of Japan Science and Technology Corporation (JST), Tokyo (Drs. Yamashita, Okamoto, Morinobu, and Yamawaki); and Hoyu Mental Hospital, Kure (Drs. Mori and Nagao), Japan.*

The authors report no financial relationships or other affiliations relevant to the subject matter of this article.

Corresponding author and reprints: Hidehisa Yamashita, M.D., Ph.D., Department of Psychiatry and Neurosciences, Graduate School of Biomedical Sciences Hiroshima University, 1-2-3, Kasumi, Minami-ku, Hiroshima 734-8551, Japan (e-mail: hidehisa@hiroshima-u.ac.jp).

One of the major symptoms of schizophrenia is sleep disturbance. Deterioration of sleep, such as prolongation of sleep latency, shortening of total sleep time, and a decrease in sleep efficiency, has been reported in patients with schizophrenia.[1] In addition, a decrease in the duration of slow wave sleep (SWS)[2] and shortened rapid eye movement (REM) latency with relatively normal REM time and density[2,3] have been demonstrated.

Sleep disturbance may exacerbate existing psychopathology by causing distress and negatively affecting general functioning in patients with schizophrenia. Decreased SWS was reported to be associated with impairment of cognitive function[4] and negative symptoms.[5] Treatment of sleep disturbance may contribute to improved quality of life in patients with schizophrenia.

Investigations of the effects of conventional antipsychotic drugs have shown that these agents could improve sleep continuity, sleep duration, and REM abnormalities, but not SWS.[6–8] The effects on sleep of atypical antipsychotic drugs could be expected to differ from those of typical antipsychotic drugs because of differences in their pharmacologic profiles. Recent pharmacologic studies of sleep revealed the importance of serotonin-2A/2C (5-$HT_{2A/2C}$) receptors on sleep quality. For example, a selective 5-$HT_{2A/2C}$ receptor antagonist, ritanserin, was reported to increase SWS in healthy volunteers[9,10] and in patients with dysthymia.[11]

Table 1. Characteristics of Schizophrenia Patients Switched From Typical to Atypical Antipsychotics

Characteristic	Total	Olanzapine	Risperidone	Perospirone	Quetiapine	p Value[b]
Age, y	59.9 ± 10.5	56.2 ± 11.2	62.8 ± 9.8	59.2 ± 8.6	61.0 ± 11.3	.22
Range	28 to 84	28 to 84	44 to 79	43 to 74	38 to 83	
Sex, male/female, N	48/44	11/9	9/11	15/9	13/15	.60
Periods of morbidity, y	34.0 ± 9.5	32.6 ± 8.7	37.6 ± 10.2	32.5 ± 9.2	33.7 ± 9.2	.26
Range	9.1 to 54.0	9.1 to 54.0	19.4 to 53.3	12.2 to 49.1	11.9 to 47.7	
Schizophrenia type, N						
Disorganized	29	7	9	2	11	.16
Paranoid	11	3	2	4	2	
Undifferentiated	52	10	9	18	15	
Dose, mean ± SD, mg/d[a]	1137 ± 981	1466 ± 984	917 ± 776	961 ± 739	1209 ± 1194	.25
Range	50 to 4383	80 to 3362	100 to 2425	88 to 3637	50 to 4383	
PSQI baseline total score, mean ± SD	8.6 ± 3.8	9.5 ± 3.0	9.1 ± 4.2	7.9 ± 3.0	8.2 ± 3.5	.47
Range	0 to 17	0 to 16	1 to 17	3 to 16	1 to 16	
PANSS baseline total score, mean ± SD	81.1 ± 15.2	82.8 ± 12.2	80.9 ± 12.9	75.1 ± 11.4	85.2 ± 19.5	.11
Range	50 to 120	60 to 108	53 to 102	54 to 109	50 to 120	
PANSS total score change, mean ± SD	−8.3 ± 7.0*	−8.3 ± 7.0*	−6.2 ± 4.7*	+2.6 ± 11.9	−4.0 ± 6.7*	
Range	−21 to 56	−21 to 2	−20 to 0	−7 to 56	−17 to 10	

[a]Converted to chlorpromazine equivalent dosage.
[b]For categorical variables (sex and type of disease), p values were obtained with the χ^2 test; for numerical variables, p values were obtained with analyses of variance.
*$p < .01$ compared with baseline; obtained with paired t test.
Abbreviations: PANSS = Positive and Negative Syndrome Scale, PSQI = Pittsburgh Sleep Quality Index.

To date, there have been several studies on the effect of atypical antipsychotic drugs on sleep. Previously, Dursun and coworkers[12] demonstrated better sleep quality in patients with schizophrenia who were treated with risperidone compared with patients receiving typical antipsychotic drugs. We reported a longer duration of SWS in patients with schizophrenia treated with risperidone than in those treated with haloperidol.[13] Acute administration of olanzapine was reported to increase sleep efficiency and SWS in drug-free patients with schizophrenia[14] and in healthy volunteers.[15] In addition, Lee and associates[16] reported that clozapine improved the continuity of sleep in schizophrenia. However, the effect of atypical antipsychotic drugs on sleep has not been compared with that of typical conventional antipsychotic drugs in the same patients with schizophrenia.

In this context, to evaluate the effect of atypical antipsychotic drugs on sleep, we compared sleep quality as measured by the Pittsburgh Sleep Quality Index (PSQI) in patients with schizophrenia while they were receiving typical conventional antipsychotic drugs and after they had been prescribed atypical antipsychotic drugs.

METHOD

Subjects

Subjects were 92 inpatients (48 men and 44 women) who had been taking conventional antipsychotic drugs only and who fully met the DSM-IV criteria for schizophrenia.[17] This study was designed in accordance with institutional guidelines and was approved by an institutional review committee. The subjects were fully informed of the purpose and procedures of the study; each subject gave written informed consent prior to enrollment. Patients were excluded if they had a severe physical illness based on results of clinical, laboratory, and imaging evaluations; a cerebral organic disease; or a history of alcoholism, drug abuse, or neurologic illness. Prior to enrollment in the study, subjects underwent medical and psychiatric screening to ensure they had no underlying cause of sleep disturbance, such as sleep apnea or restless legs syndrome. Patients who received a depot antipsychotic within 4 weeks of randomization were also excluded. Three patients had received a depot antipsychotic drug (haloperidol decanoate) before this study.

The mean age of the study population was 59.9 years (SD = 10.5, range = 28–84), and the mean duration of illness was 34.0 years (SD = 9.5, range = 9.1–54.0). The mean daily dosage of antipsychotic drug was 1137 mg/day (SD = 981, range = 50–4383) expressed as the chlorpromazine equivalent (Table 1). The mean number of antipsychotics administered at baseline was 2.2 (SD = 1.1, range = 1.0–5.0); the most common drugs were haloperidol (N = 64, 70%), chlorpromazine (N = 39, 42%), and levomepromazine (N = 23, 25%).

Treatments

After completing baseline assessments, subjects were randomly assigned to receive 1 of 4 atypical antipsychotic drugs: olanzapine (N = 20), perospirone (N = 24), quetiapine (N = 28), or risperidone (N = 20). Perospirone is a newer atypical antipsychotic agent for the treatment of schizophrenia that was developed in Japan. It was shown to have a better effect on negative symptoms and a similar effect on general and positive symptoms compared with haloperidol in phase II and phase III trials.[18]

At the time of switching, the dose of ongoing typical antipsychotics was tapered, and finally all typical antipsy-